Targeted versus whole-brain radiotherapy: systematic multiparametric and longitudinal investigations in the adult rat

Fatima-Azzahra Dwiri, Manon Audebert, Valentin Beaufils, Julie Bécam, Carole Brunaud, Jérôme Toutain, Adib Sanavi, Samuel Valable, Myriam Bernaudin, Omar Touzani, et al.

Targeted versus whole-brain radiotherapy: systematic multiparametric and longitudinal investigations in the adult rat

Fatima-Azzahra Dwiri[1], Manon Audebert[1], Valentin Beaufils[1], Julie Bécam[1], Carole Brunaud[1], Jérôme Toutain[1], Adib Sanavi[1], Samuel Valable[1], Myriam Bernaudin[1], Omar Touzani[1,2], Elodie A. Pérès[1,2*]

[1] Université de Caen-Normandie, CNRS, Normandie Université, ISTCT UMR6030, GIP Cyceron, F-14000 Caen, France

[2]Authors contributed equally to the work

*Email: peres@cyceron.fr

ABSTRACT

Although radiotherapy (RT) improves prognosis of patients with brain cancer, it induces cognitive deficits. Animal models have been employed to address the underlying mechanisms of these radiation-induced deficits. Nonetheless, in most of the animal studies, whole-brain irradiation has been applied, deviating from the clinical practice, where the goal is to reduce the exposure of healthy brain tissue to radiation. In the present study, we analyzed in the rat the evolution of brain tissue injury and cognitive impairments induced by irradiation restricted to only one cerebral hemisphere, and systematically compared them to those observed after whole-brain irradiation. Rats were divided into control (CTL), whole-brain (WBI) and hemispheric-irradiated (HBI) groups. Multiparametric magnetic resonance imaging (MRI), behavioral tests and immunohistology were performed up to six-months following the irradiation (3x10Gy). Relative to WBI, more restricted irradiation did not induce significant locomotion impairment nor anxiety-like behavior; cognitive deficits and brain atrophy were also reduced after HBI compared to WBI. MRI revealed major alterations in the microstructure and the vasculature of brain tissue in only WBI rats. However, immunohistology analyses evidenced that HBI led to persistent neuroinflammation limited to the irradiated hemisphere, which seems to be more pronounced than WBI. Overall, the data highlight that restricted brain irradiation mitigates brain damage and induces less cognitive deficits as compared to whole-brain irradiation. In the future, it is necessary to refine animal models using targeted cerebral irradiation to evaluate neuroprotective strategies.

INTRODUCTION

Radiotherapy (RT) is an essential treatment for intracranial tumors. Although RT improves the prognosis of patients, it induces collateral damage that affects cognitive abilities and quality of life in long-surviving patients. As it concerns 50 to 90% of patients treated by RT, cognition deficits in cancer care is a major concern[1–4]. The adverse effects of brain RT have been divided into 3 categories based on the time of onset of the symptoms. First, the acute side effects (fatigue, nausea) occur during or shortly after RT and are usually reversible. Second, the early delayed effects (somnolence, cognitive deficits) are typically present within 1 to 6 months post-RT. Last, the late delayed effects generally appear within months to years after RT with a progressive and irreversible cognitive decline that is often disabling[4–6]. These cognitive impairments include memory loss, deficits in attention and executive functions[4,7]. During the last decades, very substantial efforts have been made to reduce these cognitive deficits, by targeting solely the tumor area as much as possible and thus minimizing the exposure of healthy brain tissue to radiation. Thus, new RT techniques with better ballistic accuracy were developed and have been more used in clinical practice in the recent years[8]. Despite these technological advances, RT-associated cognitive deficits are still reported and unfortunately, there are no proven treatments or preventive strategies to reduce radiation toxicity in the brain[9].

Several studies based on the use of animal models have been published to analyze radiation-induced brain injury and cognitive deficits as well as their underlying mechanisms [4,10,11]. These studies suggest that brain exposure to radiation could induce vascular lesions, demyelination, inflammation, neurogenesis impairment and neurodegeneration. All these phenomena may explain cognitive dysfunctions[12–14]. Nonetheless, careful analysis of the literature shows that these animal studies are very heterogeneous in terms of animal species used, their ages and sexes as well as the dose of irradiation applied, which makes comparisons between studies very complicated to perform. Even more importantly, the vast majority of data derives from studies in which the whole brain was irradiated and one or few restricted time points of analyses were performed[4,15]. This clearly deviates from clinical reality and does not consider

all the possibilities of cerebral plasticity and inter-structure compensation that may take place following a focal irradiation-induced brain injury. Indeed, it is well known that a circumscribed lesion of brain tissue, as observed after a stroke, is accompanied by several mechanisms of cerebral plasticity, including inter-hemispheric compensation and formation of new connections between different structures. These mechanisms are thought to be involved in spontaneous functional recovery[16–18].

For many decades, radiation-based studies in laboratory animals mostly used irradiation protocols that do not conform to a single precise target. In fact, they have been limited by gross irradiation devices for clinical use. The latter deliver highly precise doses in human structures, but they entail larger dose uncertainties in the tiny structures of small animals. Indeed, animals are placed inside a uniform field and irradiated entirely; or partially by using body shielding limiting the targeted surface[19,20]. The recent technological improvement of preclinical irradiation devices offers the opportunity to researchers to extend their fields of investigations. Currently, image-guided small animal irradiators allow accurate targeting of the brain regions[21,22]. However, currently published preclinical studies on targeted irradiation are limited to irradiation of a small brain volume with a single very high dose (> 80 Gy) with the aim of mimicking hypofractionated stereotactic radiotherapy (SRT)[23–27]. Nonetheless, to date, intensity-modulated radiotherapy (IMRT) remains the most frequently used RT technique in patients treated for brain tumors. Studies on animal models of cognitive impairments induced by irradiation of larger brain tissue volumes, as observed during IMRT, are fragmentary. It is therefore necessary to conduct longitudinal and multiparametric investigations in rodents to refine the radiation-induced brain injury models to mimic, as close as possible, the most prevalent RT treatments in patients.

In the present study, using magnetic resonance imaging (MRI), behavioral tests and immunohistology, we systematically compared the effects of targeted brain irradiation and whole-brain irradiation on cognition and brain injury during a 6-month period. The first objective of this preclinical study is to provide experimental evidence for better neurocognitive

preservation after targeted irradiation, which is essential to support clinical data on the value of IMRT in reducing radiation-induced neurotoxicity. The second objective is to assess the impact of the irradiated hemisphere on the contralateral hemisphere to address the potential bystander effects and compensatory mechanisms that may take place following hemispheric brain irradiation.

Summarizing, the principal conclusion of this study confirmed that targeted irradiation strongly reduces brain damage and induces less cognitive deficits as compared to whole-brain irradiation in the rat, up to 6 months post-irradiation since no later time points were tested. The second conclusion, based on MRI and immunohistology data, is the absence of targeted brain irradiation effects on the contralateral hemisphere.

RESULTS

Animals were randomly divided into 3 experimental groups: control (CTL), hemispheric-brain irradiation (HBI) and whole-brain irradiation (WBI). Behavioral tests, MRI and immunohistology were sequentially carried out as shown on **Fig.1**. These multiparametric analyses were performed longitudinally to get closer to the temporality of appearance of the symptoms described in patients: acute (just after brain irradiation until 2 weeks), early delayed (from 1 to 3 months) and late delayed (around 6 months) effects.

Validation of the irradiation paradigm

Dosimetry. Following registration of dose deposition maps on T2-weighted images, the dose-volume histograms (DVH) were calculated in different cerebral structures following WBI or HBI. The theoretical dose received by brain structures were quantified by a treatment planning system (TPS), and were confirmed by in vivo measurements of the actual deposited dose through the use of a scintillating fiber dosimeter (DosiRat)[28]. As presented in **Fig.2a**, the dose deposition maps confirmed that all brain structures, in the case of WBI, and all hemispheric structures, in the case of HBI received doses that were close to 10 Gy at each irradiation

fraction. The D50 values for HBI and WBI were between 9.7 and 10.5 Gy in the striatum, the hippocampus and the cortex of the irradiated hemispheres. However, as awaited, rats subjected to HBI received near-zero doses in the left spared hemisphere (**Supplementary Fig.1**).

Irradiation-induced DNA damage. To ensure that the irradiation doses used were able to induce DNA damage, especially double-strand DNA breaks, brain sections were subjected to γ-H2AX staining at 2 hours after the third fraction of irradiation. HBI rats displayed an important number of γ-H2AX foci in the cortex of the right irradiated hemisphere compared to the left hemisphere and to non-irradiated control animals (**Fig.2b and 2c**). A similar pattern of expression of γ-H2AX was observed in the cortex of both hemispheres in rats that received WBI in comparison to control rats (**Fig.2b and 2c**). The subcortical structures (hippocampus, striatum) displayed similar patterns of irradiation-induced γ-H2AX expression (data not shown). Taken together, these data show that the irradiation protocols used in this study, either whole-brain or hemispheric, deliver equivalent doses with expected DNA damage in the irradiated brain areas.

Brain irradiation-induced body weight loss and death

At the beginning of the study, all animals had similar body mass (**Fig.3a**). Throughout the protocol, HBI rats exhibited a similar weight gain as that of control rats. However, WBI animals showed a significant and persistent decrease of their body mass compared to controls and HBI rats (ANOVA with Fisher's LSD tests, $p<0.0001$ at 6 months after irradiation) (**Fig.3a**).

During the 6-month period, all rats subjected to HBI survived (**Fig.3b**). Nonetheless, in the WBI group, 2 animals died at 7 days and 110 days following the irradiation respectively, the mortality rate was 17 % (**Fig.3b**). These data show that, up to 6 months, targeted irradiation had no impact on mortality rate in comparison to whole-brain irradiation.

Hemispheric or whole-brain irradiation-induced cognitive changes

Spatial learning and reference memory. During the learning phase of the Morris water maze (MWM) test, the total distance moved by the animals of the WBI group was higher in comparison to the control group at all time points (ANOVA with Fisher's LSD tests, $p<0.0001$ from 2 weeks to 5 months after irradiation) (**Fig.4a**). The rats subjected to HBI also traveled greater distances in the pool than non-irradiated control animals (ANOVA with Fisher's LSD tests, $p=0.0067$ and $p=0.0071$ at 2 weeks and 5 months, respectively), but lesser than WBI animals (ANOVA with Fisher's LSD tests, $p=0.0043$ and $p=0.0383$ at 2 weeks and 5 months, respectively). These findings suggest that HBI can alter learning capabilities, but to a lower extent in comparison to WBI.

During the probe phase of the test, both HBI and WBI animals spent less time in the target quadrant compared to CTL animals at 2 weeks after the irradiation (ANOVA with Fisher's LSD tests, $p=0.0203$ for HBI vs CTL and $p=0.0254$ for WBI vs CTL) (**Fig.4b**). Nevertheless, there were no differences between groups at the other time points studied. These data suggest that WBI and HBI alter the reference memory only at the acute phase.

Working memory. In the novel object recognition (NOR) test, we observed that HBI induced a deficit in working memory only at 6 months following the irradiation (ANOVA with Fisher's LSD tests, $p=0.0248$) (**Fig.4c**). In contrast, WBI rats showed reduced performances to recognize the novel object at the subacute and the chronic phases compared to non-irradiated rats (ANOVA with Fisher's LSD tests, $p=0.0027$ and $p<0.0001$ at 3 and 6 months, respectively). These data show that unlike WBI, HBI preserves working memory, at least during the first 5 months following the irradiation.

Long-term associative memory. The rats were submitted to the passive avoidance test at 5- and 6-month post-irradiation. In the HBI group, the animals displayed the same performances as in the CTL group (**Fig.4d**). However, WBI rats showed a reduced latency time to enter the dark compartment relative to unirradiated rats (ANOVA with Fisher's LSD tests, $p<0.0001$), which reflects a significant alteration of fear-based conditioned avoidance. These results

evidence that only WBI diminishes the long-term associative memory compared to HBI or non-irradiated animals.

Anxiety-like behavior. At 6 months following irradiation, WBI rats travelled a shorter distance in the open field (OF) and spent less time in its center compared to CTL animals (ANOVA with Fisher's LSD tests, p=0.0318) (**Fig.5a**). However, in rats subjected to HBI, there was no significant difference in comparison to the CTL group for the different parameters measured in the OF. This suggests that targeted brain irradiation has no impact on anxiety-like behavior and locomotion of rats.

In the elevated plus maze (EPM) test performed at 6 months post-irradiation, the rats subjected to WBI spent less time in the open arms compared to CTL and HBI rats (ANOVA with Fisher's LSD tests, p=0.0240 for WBI vs CTL and p=0.0211 for WBI vs HBI) (**Fig.5b**). In contrast, there was no significant difference between HBI and CTL groups whatever the EPM arm evaluated. Taken together, these data indicate that WBI, but not HBI induces anxiety-like behavior.

MRI analyses of targeted versus whole-brain irradiation-induced injury

Gross brain structure. T2-weighted images did not show any hypo- or hyper-intensities at all the time points analyzed (**Fig.6a and Supplementary Fig.2a**). This indicates that neither HBI nor WBI induced visible macroscopic necrosis or edema. However, the quantification of the cerebral volume revealed that only WBI rats displayed a significant brain atrophy at 6 months following the irradiation (6%, ANOVA with Fisher's LSD tests, p=0.0107) (**Fig.6b**). Compared to CTL group, HBI rats had a slight decrease in the whole brain volume (3%, ANOVA with Fisher's LSD tests, p=0.1539). The data show that HBI, unlike WBI, induces less cerebral atrophy.

Brain vascularization. The cerebral blood volume (CBV) was quantified by MRI in selected regions of interest (cortex, hippocampus, corpus callosum, striatum, thalamus) at 6 months after brain irradiation. Although irradiation was homogeneous throughout the brain and the right hemisphere in WBI and HBI rats respectively, the variations of CBV were distinct among

the structures analyzed (**Fig.6c**). Irrespective of the group considered, no change in CBV was noticed in the cortex and the striatum in the irradiated animals. However, we observed a decrease in CBV values in the hippocampus, the corpus callosum and the thalamus in WBI rats compared to CTL rats (ANOVA with Fisher's LSD tests, p=0.0101 for the hippocampus, p=0.0669 for the corpus callosum and p=0.0337 for the thalamus). Interestingly, no alteration of CBV values was observed in HBI irrespective of the cerebral structure considered (**Fig.6c**). These results indicate that brain structures respond differently to irradiation and that the spatial extent of irradiation determines CBV changes in different structures.

Furthermore, we analyzed the permeability of the blood-brain barrier (BBB) using dynamic contrast enhancement MRI (DCE-MRI) at 6 months post-irradiation (**Fig.7a**). Unlike T1-weighted signal in the temporal muscles, no major T1 enhancement was observed over time in the brain (**Fig.7b, 7c and 7d**) (**Supplementary Fig.2b**). The time course of the T1-weighted signal was similar between control and irradiated animals (**Fig.7b and 7c**). Thus, these MRI data show that 6 months after irradiation, both HBI and WBI models did not display brain necrosis nor permeabilization of the BBB.

Brain microstructure. To evaluate the brain microstructure and its integrity, diffusion MRI parameters were quantified in different brain areas. Mean diffusivity (MD), considered to be an indicator of edema and/or changes of cellularity, was not modified in the irradiated hemisphere in HBI animals relative to the control group (**Fig.8**) and to the non-irradiated hemisphere (data not shown), irrespective of the time point and the structure analyzed. However, in rats submitted to WBI, MD values showed a significant increase at 1 month (ANOVA with Fisher's LSD tests, p=0.0462 for the hippocampus, p=0.0188 for the corpus callosum, p<0.0001 for the striatum and the thalamus) followed by a significant decrease at 3 and 6 months following the irradiation (ANOVA with Fisher's LSD tests, p=0.0134 for the cortex, p=0.0474 for the hippocampus, p=0.0047 for the corpus callosum, p=0.0174 for the striatum and p=0.0358 for the thalamus). This pattern of irradiation-induced MD changes in WBI group was similar in all the analyzed brain regions in both irradiated hemispheres.

As for MD, radial diffusivity (RD) and axial diffusivity (AD) are putative indices of white matter integrity and cell organization in the gray matter. Generally, RD values were not significantly altered by hemispheric irradiation during all the time points analyzed, except in the cortex, corpus callosum and striatum at only 6 months after HBI (ANOVA with Fisher's LSD tests, p=0.0183 for the cortex, p=0.0055 for the corpus callosum and p=0.0334 for the thalamus) (**Supplementary Fig.3**). Likewise, HBI rats had similar AD values as CTL rats for all time points and brain structures studied (**Supplementary Fig.4**). In contrast, rats subjected to WBI displayed more extensive and persistent alterations of RD and AD values in all the brain structures examined (**Supplementary Fig.3 and Fig.4**).

Taken together, the diffusion MRI-derived data clearly shows that although WBI induces generalized and persistent microstructural brain damage, irradiation when restricted to a single hemisphere fails to cause major injury to the microstructure of the brain tissue in the rat.

Immunohistology analyses of targeted versus whole-brain irradiation-induced cellular injury

To get insights into how irradiation impacts brain tissue at the cellular level during the chronic phase (i.e., 6 months), immunohistochemistry analyses were performed to study microglia and astrocyte activation, white matter integrity, neurons and neural stem cells as well as endothelial cells.

Microglia/macrophages. Based on Iba-1 staining, we observed microglia activation as evidenced by rounded shapes of cells in both WBI and HBI rats in comparison to CTL animals (**Fig.9a**). The quantification of the positive area and the cell number confirmed this observation (**Fig.9b**, **9c and Supplementary Fig.5a**). Only in the cortex, we evidenced that HBI led to persistent microglial activation, which seems to be more pronounced than WBI (ANOVA with Fisher's LSD tests, p=0.0136 for microglia area, p=0.0309 for microglia number) (**Fig.9b**). Furthermore, microglial activation after brain irradiation was confirmed by CD68 staining which is specific to macrophages and activated microglial cells both within the cortex and the hippocampus (**Fig.9d**). Although the results were not statistically significant between the

experimental groups due to inter-animal variability, we observed a trend to an increase in the area and the cell number of CD68-positive cells in irradiated rats compared to control rats (**Fig.9e, 9f and Supplementary Fig.5b**). Based on microglia/macrophages immunohistology, the neuroinflammation appeared to be more pronounced for rats subjected to WBI than HBI.

Astrocytes. The area of GFAP-positive astrocytes as well as the cell number were significantly increased in the irradiated cortex of both HBI and WBI rats, compared to CTL animals (ANOVA with Fisher's LSD tests, for astrocyte area: p=0.0003 WBI vs CTL and p=0.0001 HBI vs CTL) (ANOVA with Fisher's LSD tests, for astrocyte number: p=0.0002 WBI vs CTL and p<0.0001 HBI vs CTL) (**Fig.10a, 10b and Supplementary Fig.5c**). Similar trends of changes were observed in the hippocampus (**Fig.10c**). These data indicate that astrogliosis was still present at 6 months after WBI or HBI, and that radiation-induced reactive astrocytes sustain an inflammatory state in the brain tissue.

White matter. The effects of whole-brain and targeted irradiation on white matter were assessed by myelin proteolipid protein (PLP) staining (**Fig.10d**). In HBI rats, no change in PLP staining was noticed in comparison to CTL rats (**Fig.10e and Supplementary Fig.5d**). However, WBI animals had a significantly reduced positive area as exemplified in the striatum compared with CTL and HBI animals (ANOVA with Fisher's LSD tests, p=0.0418 WBI vs CTL and p=0.0104 WBI vs HBI). The data evidenced that demyelination is only present in WBI rats.

Neurons and neural stem cells. We also investigated the irradiation effects on the neuronal compartment, using immunostaining of mature neurons with anti-NeuN antibody (**Fig.11a**) and neural stem cells (NSC) with anti-Sox2 antibody (**Fig.11b**). In the cortex, mature neurons and NSC were not altered by targeted or whole-brain irradiation. Indeed, the positive area and the cell number quantified from these two cell populations were similar between all animal groups (**Fig.11c and 11d**). However, in the hippocampus, the cell number of mature neurons increased (ANOVA with Fisher's LSD tests, p=0.0242 WBI vs CTL and p=0.0041 HBI vs CTL), whereas NSC tended to decrease in both HBI and WBI rats compared to CTL rats (**Fig.11e and 11f**) (**Supplementary Fig.6a and 6b**). From these data, obtained only in the delayed

phase, it could be proposed that whole-brain and targeted irradiation activate hippocampal neurogenesis with stimulation of NSC in the early phase of irradiation which may lead later to the formation of new neurons in the hippocampus.

Microvasculature. The vasculature and the permeability of the BBB were assessed, respectively, by staining a specific protein of rat endothelial cells (RECA-1) and a specific protein of tight junctions (ZO-1) in the cortex (**Fig.12a**) and the hippocampus (**Fig.12b**). As presented on **Fig.12c**, cortical vascularization was altered only after WBI since the vessel and tight junction areas were diminished only in WBI rats compared to CTL animals. Similar results were obtained for hippocampal vascularization (**Fig.12d and Supplementary Fig.6c**). Interestingly, both in the cortex and the hippocampus, we observed a significant reduction in the co-staining RECA-1/ZO-1 in only WBI rats compared to CTL rats (ANOVA with Fisher's LSD tests, for cortex: p=0.0391 WBI vs CTL and for hippocampus: p=0.0128 WBI vs CTL), revealing BBB impairments (**Fig.12c and 12d**). All data evidence that, contrary to WBI, HBI does not impact the cerebral microvasculature.

DISCUSSION

RT is an important modality for cancer treatment and remains one of the most effective tools in curing cancer. Cognitive dysfunction is one of the late effects caused by cerebral radiotherapy[4-7]. During the last decades, very substantial efforts have been made to reduce these cognitive deficits and improve the patient's quality of life, by targeting the tumor area as much as possible while minimizing the exposure of healthy brain tissue to radiation. Thus, new RT techniques with better ballistic accuracy were developed and are most commonly used in clinical practice these recent years[29,30]. Despite these technological advances, RT-associated cognitive deficits and brain injury are still reported in patients with brain metastases or primitive brain tumors[6,31–33].

Animal models of radiation-induced brain injury are relevant to determine the therapeutic gain of targeted irradiation on cerebral radiotoxicity and to study the underlying mechanisms to develop strategies to protect non-tumoral tissue. However, the literature in radiobiology is mainly focused on WBI. The animal experiments have long been performed with clinical irradiators, that do not allow to perform focal irradiation. But the recent development of irradiators dedicated to small animals offers the possibility of irradiating with several beams in different directions of space, modulating the beam intensities and having small size collimators more suitable for rodents[21,34]. Thus, it is now possible to assess the impact of focused irradiation on smaller brain volumes.

In this context, the objective of our study is to develop a targeted brain irradiation model in the rat and to assess the effects of targeted brain irradiation on cognitive outcome and cerebral tissue integrity. Thus, we compared the effects of two fractionated irradiation paradigms, with the same dose of X-rays (30 Gy) in adult rats, namely HBI and WBI. In this study, only tumor-free rats were used to avoid any confounding actions of the tumor.

The effects of WBI paradigm observed in our model, in terms of cognition or cerebral tissue damage, are concordant with several previous reports[4,6,10,35]. However, we showed that HBI did not induce weight loss and mortality as compared to WBI. Similarly, relative to WBI, more restricted irradiation did not induce significant locomotion impairment nor anxiety-like behaviors. As expected, rats subjected to WBI had cognitive deficits both in short- and long-term memory and learning abilities. Half-brain irradiation also led to learning disabilities, acute and transient reference memory deficits (only at 2 weeks post-HBI) and late working memory impairment (solely at 6 months after HBI). A slight brain atrophy was evidenced in HBI rats, but this was more pronounced after WBI. DTI-MRI and vascular MRI revealed major changes in the microstructure and the vasculature of brain tissue in WBI rats. Nonetheless, these changes were overall not found in HBI rats. As shown by immunohistochemistry, WBI induced persistent neuroinflammation, white matter disorganization, hippocampal neurogenesis modifications and vascularization damage, including BBB permeabilization, at 6 months after

irradiation. In contrast, HBI animals did not display these pathological mechanisms, except microglia activation and reactive astrogliosis that were limited to the irradiated hemisphere. All these data support that targeted brain irradiation strongly reduces brain damage and attenuates neurocognitive functions compared to WBI at least during the first 6 months.

Although, it is difficult to compare our findings with those of the literature, because of differences in dose depositions, animal species, endpoints, techniques and times of analyses employed, the observation that partial brain irradiation did not substantially modify the brain structure or function was somewhat surprising and discordant with some published studies. Based on magnetic resonance spectroscopy (MRS), Chen and collaborators showed that a HBI with a single dose of 30 Gy was able to alter the microstructure of rat brain tissue. As an example, N-acetylaspartate (NAA) was significantly reduced in irradiated semi-brain in comparison to the contralateral hemisphere, reflecting neuronal loss[36]. Another study using MRS highlighted significantly higher choline, glutamate, lactate and taurine in irradiated hemi-brain in adult rats after HBI[37]. Likewise, based on diffusion MRI, studies performed in rodents showed that targeted brain irradiation caused brain microstructure alterations sustained by MD decrease compared to the unirradiated hemisphere[38]. However, based on arterial spin labeling imaging (ASL), no significant blood perfusion changes was observed in the irradiated hemisphere at 5 Gy or 20 Gy in the mouse[38]. To further clarify the impacts of HBI on brain tissue, original imaging techniques such as functional MRI, connectivity analyses-based MRI or multimodal PET/MRI could be very relevant.

The BBB disruption and hypoperfusion are considered to be the major risk factors that contribute to the initiation and the development of radiation-induced brain injury[39,40]. In our study, we evaluated BBB impairment using DCE-MRI performed only at the end of protocol. The results obtained in the cortex and the hippocampus showed no gadolinium leakage in the brain parenchyma after WBI or HBI at 6 months after irradiation. In parallel, we used another approach to investigate BBB permeabilization based on immunohistology of tight junctions on cerebral vessels. Based on the immunostaining of RECA-1 and ZO-1 proteins, we showed that

tight junction expression in the microvasculature was significantly reduced after WBI both in the cortex and the hippocampus, demonstrating that radiation induced BBB impairment at 6 months after brain exposure to X-rays. However, ZO-1 expression was not reduced following half-brain irradiation. The divergence of available data on radiation-induced BBB alterations is not surprising as it could differ according to the methodological approaches used and the time points considered. A recent systematic review of clinical and preclinical studies on BBB permeability following radiotherapy showed that only 35% of the included clinical studies reported BBB disruption following RT, whereas preclinical studies showed BBB disruption in 78% of the included investigations[32]. This systematic review underlines the importance of RT protocols, such as fractionation schemes, cumulative doses and time points studied on BBB integrity. The difference between clinical and preclinical studies could be explained in part by the methods to investigate BBB permeability as they are limited in patients to MRI measuring the enhancement/extravasation of gadolinium, PET (^{G8}Ga-EDTA or ^{82}Rb radiotracers) and liquid chromatography–mass spectrometry (LC-MS) on cerebrospinal fluid. By contrast, there are multiple techniques in animal models such as MRI, radioactive brain uptake, chemical brain uptake, immunohistochemistry, Evans blue extravasation, intravital microscopy[32]. The invasive methods (immunohistochemistry, Evans blue extravasation, intravital microscopy) showed brain irradiation-induced BBB permeabilization for doses < 30 Gy from a few hours and days up to several months later[32,41–44]. On the contrary, non-invasive methods as the gold standard in imaging is DCE-MRI are less sensitive, since doses radiation doses between 45 Gy and 100 Gy are necessary to observe gadolinium leakage in the cerebral parenchyme[32,45–47]. Karger and colleagues demonstrated that a unique dose of 30 Gy was insufficient to detect T1-signal enhancement in the brain of rats at 19 months after irradiation. By contrast, a dose of 100 Gy induced BBB permeabilization detectable by DCE-MRI from 5 months[46].

Many preclinical studies have suggested that targeted brain irradiation causes cognitive decline but those were mainly conducted on juvenile animals. For example, irradiation targeting hippocampus during the postnatal stage in mice induced anxiety-like behavior,

memory deficits and impairments in hippocampal synaptic plasticity[48–50]. It is known that the effects of irradiation on the brain is age-dependent[15,51], and also depends on sex in animal models[52–54] as well as in humans[55,56]. Interestingly, partial brain irradiation performed in adult rodents has also been reported to induce cognitive decline when brain structures involved in neurogenesis, such as hippocampus or subventricular zone, were specifically targeted by X-rays[57,58]. Nevertheless, in these studies, the targeted brain irradiation of specific structure was bilateral (both right- and left-brain structure). Therefore, the irradiated volume could be a major parameter which influences the brain response to HBI. In fact, it is well described that the irradiated brain volume, along with the irradiation dose and fractionation scheme, is a dependent parameter in radiation-induced brain injury both in humans and rodents[56,59,60].

Radiation-induced cerebral edema and necrosis have been observed in patients and most animal models, but these are dependent on the radiation dose and the time point studied. Some preclinical studies that were performed with high doses (80 to 100 Gy) on small volumes targeting specific brain structures have reported radiation-induced necrosis associated with cognitive deficits in adult rodents[23–26]. A similar finding was reported in the mouse after a single dose of 50 Gy[44]. In our study, we elected to submit rats to WBI or HBI with a dose of 30 Gy known to be insufficient to induce tissue necrosis[10], as we confirmed with T2-weighted and T1-weighted post-gadolinium MR images. In a mouse model of WBI with a single dose of 30 Gy, there was not occurrence of apparent brain edema or radiation necrosis from 1 day up to 2 months after irradiation[41]. Furthermore, Boria and collaborators reported that mice that received 80 Gy in a single dose showed radiation-induced brain lesions, especially necrosis, dependent on the animal strain used[61].

Furthermore, by comparing HBI and WBI, the second objective of our study was to assess the impact of the irradiated hemisphere on the other brain hemisphere, and inversely, to address the potential bystander effects and compensatory mechanisms that may take place following HBI. Indeed, it is well known that a circumscribed lesion of brain tissue, as observed after stroke for example, is accompanied by several mechanisms of cerebral plasticity, including

inter-hemispheric compensation and formation of new connections between different structures. These mechanisms are thought to be involved in spontaneous functional recovery[16–18]. Our results showed no effect on the contralateral hemisphere, either by MRI or immunohistology. However, based on a stereotactic radiosurgery animal model in which highly focused X-ray beams (single dose of 10 Gy) were delivered to the hippocampus of athymic rats, Parihar and collaborators highlighted that stereotactic radiosurgery (SRS)-induced cognitive impairments were more difficult to demonstrate in animals subjected to unilateral hippocampal ablation compared to irradiation targeted both hippocampi or following whole-brain irradiation. The authors attributed these findings to compensatory increases in hippocampal neurogenesis in the contralateral side[27]. Contrarily, another study in which young adult rats were irradiated with Gamma Knife® (10 Gy) directed to the left hippocampus and shaped to minimize irradiation revealed no effect of the focal irradiation on the right hemi-brain[23]. Fan and colleagues observed that partial brain irradiation in juvenile mice induced a long-lasting impairment in neuroplasticity and microvessel network of the irradiated hippocampus, whereas the contralateral hippocampus remained unaffected[50]. Another study on juvenile mice demonstrated that radiation damage locally can have important off-target consequences, also called bystander effects, for brain development[62]. By modulating the brain structure irradiated, the researchers showed that irradiation of the anterior commissure had no impact on its volume nor on brain development compared to WBI. In contrast, HBI targeted to the olfactory bulbs or subventricular zone resulted in off-target volume reduction in the anterior commissure[62]. Moreover, although they are invasive methods, electrophysiology studies could be interesting to study excitability and synaptic plasticity. Indeed, studies in mouse models based on whole-cell recordings in hippocampal CA1 and prefrontal cortex showed that cranial irradiation impairs the intrinsic excitability and synaptic plasticity linked to cognitive deficits[63,64].

Our preclinical study presents some limitations that must be considered in the interpretation of the results and will have to be studied in future investigations. Firstly, the study was conducted on only male rats to avoid any heterogeneity that could be linked to variations in the hormonal

cycle of females. These variations may complicate the interpretation of the results of behavioral tests, especially those performed in a longitudinal manner. However, the sex is an important factor to be considered. Several studies have indeed reported that the sex of animals influences cranial irradiation-induced behavioral impairments and brain damage[54,65–67]. Therefore, for a translational relevance in brain and non-brain cancer patients treated by radiation therapy, it is important to confirm, in future experiments, these results in female animals.

Secondly, our conclusions regarding the behavior analyses can be criticized for two main reasons: the use of a battery of tests performed on consecutive days and the repetitions of the tests on the same animals over time. As described in the literature, it is possible to combine tests in rodents, but precautions must be taken to minimize stress for the animals and avoid interactions between tests[68]. We therefore performed the behavioral tests in a specific order: OF, NOR, EPM, passive avoidance and MWM. In addition, to minimize any interaction between the tests, the rats were submitted to one evaluation per day with a period of 2 weeks. On the other hand, longitudinally analyses of behavior could lead to animal habituation to the tests as well as to re-test effects which can attenuate behavioral impairments induced by treatment. As reported in the literature, the inter-test interval time is critical to lessen the re-test effects. It is recommended to use 1 week for the NOR, 4 weeks for the MWM and EPM, 24 hours for passive avoidance test[69]. In our study, we have ensured that these time intervals were respected. Furthermore, we took special care when repeating the behavioral tests to minimize the habituation of the animals. For example, the object pairs used for the NOR have been completely changed for each time point. For the MWM, the location of the platform within the pool as well as the visual cues on the walls of the testing room were changed every time.

Finally, our longitudinal study was performed up to 6 months after brain irradiation. This duration of experimental protocol was chosen to get closer to the temporality of appearance of the symptoms described by the patients: acute (just after brain irradiation until 2 weeks), early delayed (from 1 to 3 months) and late delayed (around 6 months) effects. Taken together, our

results showed that the targeted irradiation in the rat strongly reduced brain tissue damage and attenuated cognitive deficits as compared to WBI. It is important to stress that this conclusion only covers up to 6 months post-irradiation since no further time points were tested. Future studies at later time points (one year and beyond) may be relevant to determine whether HBI induces delayed effects.

To conclude, through a systematic and longitudinal comparison with WBI, we highlighted that HBI mitigated brain tissue damage and attenuated neurocognitive deficits in adult rats up to 6 months after irradiation compared to WBI. Considering the RT modalities used in patients with brain tumors, our animal model of targeted cerebral irradiation could be a great interest in refining the animal models of radiation-induced brain injury to be adapted to the cranial irradiation practiced in patients. Moreover, the use of an animal model based on targeted brain irradiation would be more relevant for the development and validation of neuroprotective strategies.

METHODS

Animals and experimental design

The study was performed using 5-months-old male Wistar rats (Janvier Labs) and followed up to 6 months. Rats were housed in climate- and light-controlled conditions (temperature of 22-24°C, 12/12-hour light/dark cycle). Animals were randomly divided into 3 experimental groups: control (CTL, n=16), hemispheric-brain irradiation (HBI, n=14) and whole-brain irradiation (WBI, n=12). These animal studies have been approved by the appropriate ethics committee and have therefore been performed in accordance with the ethical standards laid down in the 1964 Declaration of Helsinki and its later amendments. Animal investigations performed in this study is in accordance with the current European directive (2010/63/EU). Ethical approval was obtained from the regional committee (CENOMEXA) and the French Ministère de l'Enseignement Supérieur, de la Recherche et de l'Innovation (APAFIS #24072). Behavioral

tests, magnetic resonance imaging (MRI) and immunohistology have been performed as shown on **Fig.1**.

Brain irradiation procedures

The irradiation was performed with X-RAD 225Cx, a small-animal irradiator associated to cone beam computed tomography (CBCT) for image-guidance (Precision X-ray, CYCERON). The protocols of irradiation were defined using a Treatment Planning System (TPS) based on SmART-Plan software[70]. To confirm the precision of TPS, the actual doses absorbed by the brain were measured by an *in vivo* dosimetry based on a scintillating fiber dosimeter, called DosiRat[28]. Moreover, dosimetry analyses were performed in the irradiator before beginning the animal study. The reference dose measurement was done using an ionization chamber (Farmer PTW 30013) calibrated in air kerma. Then, dose measurements in air and inside the brain of dead rats were performed using a scintillating fiber detector used by medical physicists for dosimetry verifications of clinical irradiators (Exradin W1 scintillator). From the theoretical dose fixed to 10 Gy for one irradiation fraction with TPS, we measured actual dose of 9.99 Gy for WBI and 9.88 Gy for HBI with scintillating fiber detector. The coefficient of variation between WBI and HBI protocols defined with same irradiation configuration (X-ray beam delivered from the top to the bottom of the head) was 1.16% which shows a negligible variation between the 2 irradiation processes, since the measurement certainties are conventionally fixed at 5%.

Rats were anesthetized with 2.5% isoflurane in 30% O_2 / 70% N_2O. To avoid any anesthesia bias, the CTL animals n=16) were anesthetized similarly as the irradiated ones. The whole-brain (WBI, n=12) or right hemisphere of the brain (HBI, n=14) (except the cerebellum and olfactory bulbs) were irradiated using a circular collimator of Ø25 mm and Ø15 mm, respectively. A total dose of 30 Gy was delivered in 3 fractions (10 Gy per day during 3 consecutive days at a dose rate of 3.3 Gy/min). In this study, the time day 0 (noted D0) corresponded to the last irradiation fraction with total dose delivered (**Fig.1**). The irradiation dose was chosen to have a translational relevance by ensuring that the pathophysiology

induced after cranial irradiation is relatively similar between rats and humans. Indeed, a minimum dose of 30 Gy is required in rats to induce vascular damage and demyelination without white matter necrosis[10,71,72]. Those phenomena are the main radiation-induced brain injuries associated to cognitive deficits in brain tumors patients treated by radiotherapy (RT)[73,74].

The X-ray beam characteristics were: voltage=225 kV, intensity=13 mA, energy=80 keV, 1mm Cu filter. The Source Skin Distance (SSD) was about 30 cm. It slightly varied between animals. Indeed, the positioning of the animal relative to the X-ray beam was precisely adapted by positioning the irradiation target on the entire brain or only the right hemisphere according to the CBCT-scan images obtained for each rat and each irradiation fraction. For information, the current small animal image-guided radiotherapy is based on the use of orthovoltage irradiator[21,22]. Although these preclinical irradiators are more suitable for studies of cerebral radiotoxicity in rodents, it is necessary to collimate the X-ray beam to precisely irradiate only the brain and to use a copper filter for only letting through hard X-rays and ensure optimal absorption of X-rays in brain depth.

After the irradiation procedure and recovery from anesthesia, rats returned to their home cages. The animals were then monitored daily until the end of the study.

Behavioral analyses

All behavioral tests were performed and analyzed by the same experimenter according to the schedule presented on **Fig.1**. The randomization of animals was realized for each behavioral test and all time points, and all analyses were performed in a blind manner. A battery of behavioral tests was performed at 1 week, 2 weeks, 2 months, 3 months, 5 months and 6 months after cerebral irradiation to assess memory, learning, locomotion and anxiety. The number of animals differed depending on the behavioral tests, the times studied and the experimental groups (CTL: n_{max}=15 – n_{min}=9 / HBI: n_{max}=14 – n_{min}=7 / WBI: n_{max}=11 – n_{min}=9). According to the time pointstudied after irradiation, the tests were performed in a specific order

to minimize the stress for the animals and avoid interactions between the tests: OF, NOR, EPM, passive avoidance and MWM. In addition, only one test was realized per day and they were spread over a period of 2 weeks.

Novel Object Recognition. This test was performed to assess short-term working memory[75,76]. Briefly, 24 h before the test, each rat was allowed to familiarize itself with a rectangular 65x45x45 cm wooden dark OF during 10 min. On the testing day, the rat was placed in the OF and left 2 min to explore it, then 2 identical objects (familiar) were placed in the OF and the rat was allowed to explore them during 5 min. The animal was then placed back into his cage for 2 min. The objects were once again cleaned and one was placed back (familiar) with a new one (novel). The rat was again placed in the OF and left to explore the two objects within 5 min. To avoid habituation of animals to test repetition during the experimental protocol, the object pairs used have been completely changed for each time studied after irradiation. From the videos acquired during all phases of the test, the exploration time for each object was determined by *a posteriori* analysis and realized manually. The recognition Index (RI) was calculated as the ratio between the time spent exploring the novel object and the time spent exploring both objects.

Morris Water Maze. This task was used to assess spatial learning and reference memory according to the standard protocol[77]. Briefly, rats were tested in a circular pool filled with opaque water. The training phase was performed during 4 successive days, in which a platform was hidden underwater. The rats were required to find the submerged platform within 90 sec, using visual cues on the walls of the testing room, and all the rats performed 4 successive trials per day. To evaluate spatial learning, the distance traveled to find the platform was measured. The probe test was made at day 5: the platform was removed and the rats were allowed to swim freely for 60 sec. To avoid habituation of animals to the test repetition during the experimental protocol, the location of the platform within the pool as well as the visual cues on the walls of the testing room were changed every time. The time spent in the target quadrant

was measured. Data were recorded using the video-tracking software VideoTrack (Viewpoint) and automatically analyzed using EthoVision XT-14 software (Noldus).

Passive Avoidance. The fear-motivated test was used to assess fear-based conditioned avoidance long-term associative memory[78]. The apparatus is composed of a 2-compartment box: a lighted compartment connected to a smaller dark compartment by a door (Bioseb). At the beginning of the test, each rat was placed in the lightened compartment for 30 sec, then the door was automatically opened, and as soon as the animal entered the dark compartment, it received an electrical foot shock (0.6 mA during 1 sec). The rat was then placed back to its cage until the retention trial performed 24 h after acquisition phase. The acquisition and retention phases were carried out at 11 days before the irradiation whereas only the retention trial was performed after the irradiation. The latency time for entering the dark compartment was measured. From the videos acquired during the test, the latency time was determined by a posteriori analysis and realized manually.

Open field. Anxiety-like behavior and locomotion were evaluated by the OF task using a 1x1x0.6 m white square box[79]. For 10 minutes, rats were always placed in the lower left corner of the apparatus. The time spent in the center, in the periphery and the total distance moved by the animals were automatically quantified by the video-tracking software VideoTrack (Viewpoint) and *a posteriori* analyzed using EthoVision XT-14 software (Noldus).

Elevated-Plus Maze. This test was used to assess anxiety-like behaviors[80]. The apparatus is a cross-shaped platform constituted of 4 arms[81]. Briefly, the 2 opposite arms were enclosed by side and end walls and the 2 other opposite arms were open. The connecting open center allows the rat to move from one arm to another. The animals, while being filmed, were allowed to explore freely during 5 min. The videos were automatically analyzed using the video-tracking EthoVision XT-14 software (Noldus) to measure the time spent in the center, open and closed arms.

Magnetic resonance imaging

595 Multiparametric cerebral MRI was realized at 1 month, 3 months and 6 months after irradiation
596 to non-invasive investigate the brain macrostructure, the microstructure integrity and the brain
597 vascularization. Imaging studies were always done after the behavioral tests to avoid bias
598 related to the gas anesthesia required for MRI acquisitions. The number of animals for MRI
599 was the same for all times studied as indicated below: CTL: n=9, HBI: n=11 and WBI: n=10.
600 The randomization of animals was realized for each imaging time point and all analyses were
601 blindly performed.

602 **MRI examinations.** MRI (7-Tesla PharmaScan®, Bruker BioSpin, CYCERON) was performed
603 at different time points. Rats were anesthetized with 2% isoflurane in 30% O_2 / 70% N_2O. Their
604 respiratory rate was monitored and their body temperature was maintained around 37 °C. The
605 following sequences were acquired: (1) T2-weighted RARE imaging: factor RARE = 4, TR/TE_{eff}
606 = 5000/30 ms, average = 1, repetitions = 2, 64 contiguous slices, spatial resolution = 0.125 x
607 0.125 x 0.5 mm^3; acquisition time = 8 min; (2) DTI imaging: TR/TE = 2192/37 ms, 30 directions
608 and 2 b-values = 0 and 1000 s/mm^2, A0 images = 5, average = 1, repetitions = 3, 32 contiguous
609 slices, spatial resolution = 0.167x 0.167 x 1 mm^3; acquisition time = 15 min; (3) T2star EPI
610 acquisitions: TR/TE = 20000/13 ms, average = 1, repetition = 6, 32 contiguous slices, spatial
611 resolution = 0.290 x 0.290 x 1 mm^3; acquisition time = 2 min and (4) Dynamic contrast
612 enhanced (DCE)-MRI with multiple T1-weighted imaging from SE sequence: TR/TE = 203/3.5
613 ms, average = 1, repetitions = 12, interval repetition = 45 s, 24 contiguous slices, spatial
614 resolution = 0.167 x 0.167 x 1.5 mm^3; acquisition time = 8 min. T2 star were acquired before
615 and 4 min after P904 contrast agent injection (Chematech; 200 µmol/kg). For DCE-MRI, after
616 the acquisition of 2 baseline T1-weighted (T1w) images, a bolus of gadolinium (Dotarem®; 200
617 µmol/kg) was injected through the tail vein.
618 From Paravision 6.0 software, the following diffusion images were reconstructed: mean
619 diffusivity (MD) = (λ1+λ2+λ3)/3; axial diffusivity (AD) = λ1 and radial diffusivity (RD) = (λ2+λ3)/2.
620 Cerebral blood volume (CBV) maps were generated using a homemade macro from ImageJ
621 software[82] and determined by the Steady-State method as previously described[83].

MRI analyses. From T2-weighted images, brain was subsequently masked using the BrainSuite software[84] and then the total brain volume was quantified with the ImageJ software as previously detailed[85].

The first step for processing DTI or T2star images consisted in registering the A0 images of each animal on a homemade template using the Advanced Normalization Tools (ANTs)[86]. After the registration by non-linear transformation, the transformation matrix obtained for each rat was applied to the different diffusion parameter maps studied (MD, AD and RD) or CBV maps. DCE-MRI was used to estimate vascular permeability by measuring gadolinium leakage through the blood-brain barrier (BBB). Time-course curves of T1-weighted signal were extracted in the cortex, the hippocampus and the temporal muscles using ImageJ software. The T1-signal enhancement for each animal was quantified by a normalization of the signal relative to the first acquisition without gadolinium.

Immunohistochemistry

Two hours or six months post-irradiation, rats received 0.05 mg/Kg of buprenorphine (Buprécare®, Axience, sc) 30 min before being deeply anesthetized with 5% isoflurane in 30% O_2 and 70% N_2O. The animals underwent a transcardiac perfusion with cold heparinized saline solution and the brains were immediately removed and immersed in a paraformaldehyde solution (PFA 4%) during 24 h. Coronal sections (30 µm) were cut using a freezing microtome.

Immunohistology analyses were performed 2 hours after the last fraction of irradiation to investigate DNA damage, and at the end of experimental protocol (i.e., 6 months after irradiation) to study the different cerebral cell populations. Each immunostaining was blindly performed on 3 rats for each experimental group.

Several primary antibodies were used to characterize DNA double-strand breaks with γ-H2Ax (1:200; 2577S; Cell Signaling), microglia with ionized calcium-binding adaptor molecule 1 (Iba-1) (1:100; ab5076; Abcam), macrophages with cluster of differentiation 68 (CD68) (1:100; MAB1435; Merck), astrocytes with glial fibrillary acidic protein (GFAP) (1:500; Z0334; Dako),

white-matter with myelin proteolipid protein (PLP) (1:500; ab28486; Abcam), neurons with neuronal nuclei (NeuN) (1:500; MAB377, Merck), neural stem cells with sex determining region Y-box 2 (Sox2) (1:1000; ab97959; Abcam), vessels with rat endothelial cell antigen-1 (RECA-1) (1:100; MCA970R; Bio-rad) and endothelial tight junctions with zonula occludens-1 (ZO-1) (1:100; 402200; Invitrogen). Before staining, non-specific binding sites were blocked with 3% of bovine serum albumin (BSA) with 0.1% Tween / 0.5% Triton in PBS solution for 2h at room temperature. The brain slices were then incubated with primary antibodies in 1% BSA / 0.1% Tween / 0.5% Triton in PBS at 4°C overnight. The staining was revealed by a fluorochrome-conjugated secondary antibodies Alexa Fluor 488 and 555 (1:500; Abcam) co-incubated with Hoechst 33342 (1:1000; Sigma-Aldrich®) for nuclei staining. Brain sections were examined with a Leica DMi8 microscope and images were separately acquired in right (ipsilateral) and left (contralateral) hemispheres.

All immunostainings were blindly quantified from ImageJ software. Briefly, a threshold determined from fluorescence intensity was fixed to obtained mask of each image, and next the positive area and cell number were quantified with ImageJ macro “Analyze particle”.

Statistical analyses

All data are presented as mean + standard deviation (SD). Statistical analyses, one-way or two-way ANOVA followed with LSD Fisher’s post-hoc, were performed with GraphPad Prism® software (version 9.3.1.471). The number of animals in each experiment is stated in the corresponding figure legend.

Data availability

The data from this study are tabulated in the main paper and supplementary materials. The research data are stored in an institutional repository and will be shared upon reasonable request to the corresponding author.

Reporting summary. Further information on research design is available in the Nature Portfolio Reporting Summary linked to this article.

Acknowledgments

The authors thank the Behavioral Research Platform (BRP, UNICAEN, France), the CYCERON Platform, the Centre Universitaire de Ressources Biologiques (CURB) for animal accommodation and Anne-Marie Frelin (Grand Accélérateur National d'Ions Lourds - GANIL, Caen, France) for control quality of irradiation and dosimetry checking with the scintillating fiber dosimeter. This work was partly performed on a facility (CYCERON platform) of France Life Imaging network (grant ANR-11- INBS-0006).

This study was supported by co-funding from the Région Normandie, the European Union-Fonds Européen de Développement Régional (FEDER), the French State in the framework of the interregional development Contract « Vallée de la Seine » 2015-20 (RIN Habionor), 2018-21 (RIN 3R) and 2019-22 (RIN Cancer-Cog), the CNRS, the GDR Sport et Activité Physique, the Université de Caen-Normandie, the Ministère de l'Enseignement Supérieur et de la Recherche and the French National Agency for Research « Investissement d'Avenir » (n°ANR-10-EQPX1401), Archade and the Cancéropôle Nord-Ouest.

Author contributions

F.A.D. conducted all the experiments, performed data analyses and wrote the manuscript; M.A. contributed to immunohistological studies and wrote the revised manuscript, V.B. contributed to irradiation experiments, validation of behavioral tests, discussed experiments and wrote the revised manuscript, J.B. contributed to irradiation experiments, validation of behavioral tests and discussed experiments; C.B. performed pre-processing MRI images and analyzed MRI data, J.T. contributed to irradiation experiments and MRI acquisitions, A.S. contributed to MRI analyses; S.V. provided funding and discussed experiments, M.B. provided funding and discussed experiments, O.T. supervised the research, provided funding, wrote the

manuscript and its revised version, E.A.P. supervised the research, provided funding, wrote the manuscript and its revised version. All the authors have read and revised the manuscript.

Competing interests

The authors declare no competing interests.

Publisher's note: Springer Nature remains neutral with regard to jurisdictional claims in published maps and institutional affiliations.

Peer review information: Lab Animal thanks….

REFERENCES

1. Wilke, C., Grosshans, D., Duman, J., Brown, P. & Li, J. Radiation-induced cognitive toxicity: Pathophysiology and interventions to reduce toxicity in adults. *Neuro-Oncol.* (2017) doi:10.1093/neuonc/nox195.
2. Lawrie, T. A. *et al.* Long-term neurocognitive and other side effects of radiotherapy, with or without chemotherapy, for glioma. *Cochrane Database Syst. Rev.* **8**, CD013047 (2019).
3. Acevedo-Vergara, K. *et al.* Cognitive deficits in adult patients with high-grade glioma: A systematic review. *Clin. Neurol. Neurosurg.* **219**, 107296 (2022).
4. Perez, W. D. & Perez-Torres, C. J. Neurocognitive and radiological changes after cranial radiation therapy in humans and rodents: a systematic review. *Int. J. Radiat. Biol.* **99**, 119–137 (2023).
5. Greene-Schloesser, D. *et al.* Radiation-induced brain injury: A review. *Front. Oncol.* **2**, 73 (2012).
6. Makale, M. T., McDonald, C. R., Hattangadi-Gluth, J. A. & Kesari, S. Mechanisms of radiotherapy-associated cognitive disability in patients with brain tumours. *Nat. Rev. Neurol.* **13**, 52–64 (2017).

7. Jalali, R. *et al.* Efficacy of Stereotactic Conformal Radiotherapy vs Conventional Radiotherapy on Benign and Low-Grade Brain Tumors: A Randomized Clinical Trial. *JAMA Oncol.* **3**, 1368–1376 (2017).
8. Matsui, J. K. *et al.* Advances in Radiotherapy for Brain Metastases. *Surg. Oncol. Clin. N. Am.* **32**, 569–586 (2023).
9. Jacob, J. *et al.* Cognitive impairment and morphological changes after radiation therapy in brain tumors: A review. *Radiother. Oncol. J. Eur. Soc. Ther. Radiol. Oncol.* **128**, 221–228 (2018).
10. Yang, L. *et al.* Pathophysiological Responses in Rat and Mouse Models of Radiation-Induced Brain Injury. *Mol. Neurobiol.* **54**, 1022–1032 (2017).
11. Li, Z. *et al.* Application of Animal Models in Cancer Research: Recent Progress and Future Prospects. *Cancer Manag. Res.* **Volume 13**, 2455–2475 (2021).
12. Lumniczky, K., Szatmári, T. & Sáfrány, G. Ionizing Radiation-Induced Immune and Inflammatory Reactions in the Brain. *Front. Immunol.* **8**, 517 (2017).
13. Pazzaglia, S., Briganti, G., Mancuso, M. & Saran, A. Neurocognitive Decline Following Radiotherapy: Mechanisms and Therapeutic Implications. *Cancers* **12**, 146 (2020).
14. Bálentová, S. *et al.* Effect of whole-brain irradiation on the specific brain regions in a rat model: Metabolic and histopathological changes. *Neurotoxicology* **60**, 70–81 (2017).
15. Tomé, W. A. *et al.* Hippocampal-dependent neurocognitive impairment following cranial irradiation observed in pre-clinical models: current knowledge and possible future directions. *Br. J. Radiol.* **89**, 20150762 (2016).
16. Kane, E. & Ward, N. S. Neurobiology of Stroke Recovery. in *Clinical Pathways in Stroke Rehabilitation: Evidence-based Clinical Practice Recommendations* (ed. Platz, T.) (Springer, Cham (CH), 2021).
17. Silasi, G. & Murphy, T. H. Stroke and the connectome: how connectivity guides therapeutic intervention. *Neuron* **83**, 1354–1368 (2014).

18. Van der Linden, A. & Hoehn, M. Monitoring Neuronal Network Disturbances of Brain Diseases: A Preclinical MRI Approach in the Rodent Brain. *Front. Cell. Neurosci.* **15**, 815552 (2021).
19. Khan, M. A., Hill, R. P. & Van Dyk, J. Partial volume rat lung irradiation: an evaluation of early DNA damage. *Int. J. Radiat. Oncol. Biol. Phys.* **40**, 467–476 (1998).
20. Bálentová, S. *et al.* Radiation-induced long-term alterations in hippocampus under experimental conditions. *Klin. Onkol. Cas. Ceské Slov. Onkol. Spolecnosti* **25**, 110–116 (2012).
21. Verhaegen, F. *et al.* ESTRO ACROP: Technology for precision small animal radiotherapy research: Optimal use and challenges. *Radiother. Oncol. J. Eur. Soc. Ther. Radiol. Oncol.* **126**, 471–478 (2018).
22. Brown, K. H. *et al.* A scoping review of small animal image-guided radiotherapy research: Advances, impact and future opportunities in translational radiobiology. *Clin. Transl. Radiat. Oncol.* **34**, 112–119 (2022).
23. Schindler, M. K., Bourland, J. D., Forbes, M. E., Hua, K. & Riddle, D. R. Neurobiological responses to stereotactic focal irradiation of the adult rodent hippocampus. *J. Neurol. Sci.* **306**, 129–137 (2011).
24. Hideghéty, K. *et al.* Development of a small-animal focal brain irradiation model to study radiation injury and radiation-injury modifiers. *Int. J. Radiat. Biol.* **89**, 645–655 (2013).
25. Constanzo, J. *et al.* Diffusion MRI monitoring of specific structures in the irradiated rat brain. *Magn. Reson. Med.* **80**, 1614–1625 (2018).
26. Constanzo, J. *et al.* Brain irradiation leads to persistent neuroinflammation and long-term neurocognitive dysfunction in a region-specific manner. *Prog. Neuropsychopharmacol. Biol. Psychiatry* **102**, 109954 (2020).
27. Parihar, V. K. *et al.* Defining functional changes in the brain caused by targeted stereotaxic radiosurgery. *Transl. Cancer Res.* **3**, 124–137 (2014).

28. Le Deroff, C., Pérès, E. A., Ledoux, X., Toutain, J. & Frelin-Labalme, A.-M. In vivo surface dosimetry with a scintillating fiber dosimeter in preclinical image-guided radiotherapy. *Med. Phys.* **47**, 234–241 (2020).
29. Diehl, C. & Combs, S. E. Modern Techniques of Radiation Therapy in the Treatment of Brain Tumors and Tumors of the Skull Base. *Neurol. Int. Open* **2**, E97–E107 (2018).
30. Scaringi, C., Agolli, L. & Minniti, G. Technical Advances in Radiation Therapy for Brain Tumors. *Anticancer Res.* **38**, 6041–6045 (2018).
31. Lehrer, E. J. *et al.* The Cognitive Effects of Radiotherapy for Brain Metastases. *Front. Oncol.* **12**, 893264 (2022).
32. Hart, E. *et al.* Blood-brain barrier permeability following conventional photon radiotherapy - A systematic review and meta-analysis of clinical and preclinical studies. *Clin. Transl. Radiat. Oncol.* **35**, 44–55 (2022).
33. Garsa, A. *et al.* Radiation Therapy for Brain Metastases: A Systematic Review. *Pract. Radiat. Oncol.* **11**, 354–365 (2021).
34. Brown, K. H. *et al.* A scoping review of small animal image-guided radiotherapy research: Advances, impact and future opportunities in translational radiobiology. *Clin. Transl. Radiat. Oncol.* **34**, 112–119 (2022).
35. Tomé, W. A. *et al.* Hippocampal-dependent neurocognitive impairment following cranial irradiation observed in pre-clinical models: current knowledge and possible future directions. *Br. J. Radiol.* **89**, 20150762 (2016).
36. Chen, H., Cheng, Y.-S. & Zhou, Z.-R. Long-term Brain Tissue Monitoring after Semi-brain Irradiation in Rats Using Proton Magnetic Resonance Spectroscopy: A Preliminary Study In vivo. *Chin. Med. J. (Engl.)* **130**, 957–963 (2017).
37. Chan, K. C. *et al.* MRI of late microstructural and metabolic alterations in radiation-induced brain injuries. *J. Magn. Reson. Imaging JMRI* **29**, 1013–1020 (2009).
38. Kovács, N. *et al.* Multimodal PET/MRI Imaging Results Enable Monitoring the Side Effects of Radiation Therapy. *Contrast Media Mol. Imaging* **2018**, 5906471 (2018).

809 39. Cao, Y. *et al.* Dynamic contrast-enhanced magnetic resonance imaging as a biomarker for
810 prediction of radiation-induced neurocognitive dysfunction. *Clin. Cancer Res. Off. J. Am.*
811 *Assoc. Cancer Res.* **15**, 1747–1754 (2009).
812 40. Xie, Y., Huang, H., Guo, J. & Zhou, D. Relative cerebral blood volume is a potential
813 biomarker in late delayed radiation-induced brain injury. *J. Magn. Reson. Imaging JMRI*
814 **47**, 1112–1118 (2018).
815 41. He, Y. *et al.* Utilizing the Faxitron MultiRad 225 X-ray irradiation system for the construction
816 of mouse chronic whole brain radiation model. *J. Radiat. Res. (Tokyo)* rrab086 (2021)
817 doi:10.1093/jrr/rrab086.
818 42. Yuan, H. *et al.* Effects of fractionated radiation on the brain vasculature in a murine model:
819 Blood–brain barrier permeability, astrocyte proliferation, and ultrastructural changes. *Int.*
820 *J. Radiat. Oncol.* **66**, 860–866 (2006).
821 43. Cheng, J. *et al.* A phase 2 study of thalidomide for the treatment of radiation-induced blood-
822 brain barrier injury. *Sci. Transl. Med.* **15**, eabm6543 (2023).
823 44. Shi, Z. *et al.* Microglia drive transient insult-induced brain injury by chemotactic recruitment
824 of CD8+ T lymphocytes. *Neuron* **111**, 696-710.e9 (2023).
825 45. Münter, M. W. *et al.* Delayed vascular injury after single high-dose irradiation in the rat
826 brain: histologic immunohistochemical, and angiographic studies. *Radiology* **212**, 475–482
827 (1999).
828 46. Karger, C. P. *et al.* Dose-response curves and tolerance doses for late functional changes
829 in the normal rat brain after stereotactic radiosurgery evaluated by magnetic resonance
830 imaging: influence of end points and follow-up time. *Radiat. Res.* **157**, 617–625 (2002).
831 47. Suckert, T. *et al.* Late Side Effects in Normal Mouse Brain Tissue After Proton Irradiation.
832 *Front. Oncol.* **10**, 598360 (2020).
833 48. Dos Santos, M. *et al.* Development of whole brain versus targeted dentate gyrus irradiation
834 model to explain low to moderate doses of exposure effects in mice. *Sci. Rep.* **8**, 17262
835 (2018).

49. Serrano, C. *et al.* Targeted Dorsal Dentate Gyrus or Whole Brain Irradiation in Juvenile Mice Differently Affects Spatial Memory and Adult Hippocampal Neurogenesis. *Biology* **10**, 192 (2021).
50. Fan, H. *et al.* Partial-Brain Radiation-Induced Microvascular Cognitive Impairment in Juvenile Murine Unilateral Hippocampal Synaptic Plasticity. *Int. J. Radiat. Oncol. Biol. Phys.* **112**, 747–758 (2022).
51. Schindler, M. K., Forbes, M. E., Robbins, M. E. & Riddle, D. R. Aging-dependent changes in the radiation response of the adult rat brain. *Int. J. Radiat. Oncol. Biol. Phys.* **70**, 826–834 (2008).
52. Kovalchuk, A. *et al.* Profound and Sexually Dimorphic Effects of Clinically-Relevant Low Dose Scatter Irradiation on the Brain and Behavior. *Front. Behav. Neurosci.* **10**, 84 (2016).
53. Perez, E. C. *et al.* Olfactory Memory Impairment Differs by Sex in a Rodent Model of Pediatric Radiotherapy. *Front. Behav. Neurosci.* **12**, 158 (2018).
54. Hinkle, J. J., Olschowka, J. A., Love, T. M., Williams, J. P. & O'Banion, M. K. Cranial irradiation mediated spine loss is sex-specific and complement receptor-3 dependent in male mice. *Sci. Rep.* **9**, 18899 (2019).
55. Bleyer, W. A. *et al.* Influence of age, sex, and concurrent intrathecal methotrexate therapy on intellectual function after cranial irradiation during childhood: a report from the Children's Cancer Study Group. *Pediatr. Hematol. Oncol.* **7**, 329–338 (1990).
56. Lawrence, Y. R. *et al.* Radiation dose-volume effects in the brain. *Int. J. Radiat. Oncol. Biol. Phys.* **76**, S20-27 (2010).
57. Feierstein, C. E. *et al.* Disruption of Adult Neurogenesis in the Olfactory Bulb Affects Social Interaction but not Maternal Behavior. *Front. Behav. Neurosci.* **4**, 176 (2010).
58. Ngen, E. J. *et al.* A preclinical murine model for the early detection of radiation-induced brain injury using magnetic resonance imaging and behavioral tests for learning and memory: with applications for the evaluation of possible stem cell imaging agents and therapies. *J. Neurooncol.* **128**, 225–233 (2016).

59. Münter, M. W. *et al.* Delayed Vascular Injury after Single High-Dose Irradiation in the Rat Brain: Histologic, Immunohistochemical, and Angiographic Studies. *Radiology* **212**, 475–482 (1999).
60. Alexandrovna, Z. Y. *et al.* Radiation-Induced Cognitive Dysfunction After Different Schemes of Fractionated Whole Brain Irradiation. *Neurosci. Int.* **5**, 26–35 (2015).
61. Boria, A. J. & Perez-Torres, C. J. Impact of mouse strain and sex when modeling radiation necrosis. *Radiat. Oncol. Lond. Engl.* **15**, 141 (2020).
62. Beera, K. G. *et al.* Altered brain morphology after focal radiation reveals impact of off-target effects: implications for white matter development and neurogenesis. *Neuro-Oncol.* **20**, 788–798 (2018).
63. Wu, M.-Y. *et al.* Cranial irradiation impairs intrinsic excitability and synaptic plasticity of hippocampal CA1 pyramidal neurons with implications for cognitive function. *Neural Regen. Res.* **17**, 2253–2259 (2022).
64. Zhang, D. *et al.* Radiation induces age-dependent deficits in cortical synaptic plasticity. *Neuro-Oncol.* **20**, 1207–1214 (2018).
65. Perez, E. C. *et al.* Olfactory Memory Impairment Differs by Sex in a Rodent Model of Pediatric Radiotherapy. *Front. Behav. Neurosci.* **12**, 158 (2018).
66. Kovalchuk, A. *et al.* Profound and Sexually Dimorphic Effects of Clinically-Relevant Low Dose Scatter Irradiation on the Brain and Behavior. *Front. Behav. Neurosci.* **10**, 84 (2016).
67. Schindler, M. K., Forbes, M. E., Robbins, M. E. & Riddle, D. R. Aging-dependent changes in the radiation response of the adult rat brain. *Int. J. Radiat. Oncol. Biol. Phys.* **70**, 826–834 (2008).
68. Jaehne, E. J., Corrone, M. & van den Buuse, M. Administering a Behavioral Test Battery in Rodents. *Methods Mol. Biol. Clifton NJ* **2746**, 87–100 (2024).
69. Cnops, V., Iyer, V. R., Parathy, N., Wong, P. & Dawe, G. S. Test, rinse, repeat: A review of carryover effects in rodent behavioral assays. *Neurosci. Biobehav. Rev.* **135**, 104560 (2022).

70. van Hoof, S. J., Granton, P. V. & Verhaegen, F. Development and validation of a treatment planning system for small animal radiotherapy: SmART-Plan. *Radiother. Oncol. J. Eur. Soc. Ther. Radiol. Oncol.* **109**, 361–366 (2013).
71. Brown, W. R. *et al.* Capillary loss precedes the cognitive impairment induced by fractionated whole-brain irradiation: A potential rat model of vascular dementia. *J. Neurol. Sci.* **257**, 67–71 (2007).
72. Panagiotakos, G. *et al.* Long-Term Impact of Radiation on the Stem Cell and Oligodendrocyte Precursors in the Brain. *PLoS ONE* **2**, e588 (2007).
73. Huynh-Le, M.-P. *et al.* Microstructural Injury to Corpus Callosum and Intrahemispheric White Matter Tracts Correlate With Attention and Processing Speed Decline After Brain Radiation. *Int. J. Radiat. Oncol. Biol. Phys.* **110**, 337–347 (2021).
74. Farjam, R. *et al.* A Radiation-Induced Hippocampal Vascular Injury Surrogate Marker Predicts Late Neurocognitive Dysfunction. *Int. J. Radiat. Oncol. Biol. Phys.* **93**, 908–915 (2015).
75. Bevins, R. A. & Besheer, J. Object recognition in rats and mice: a one-trial non-matching-to-sample learning task to study 'recognition memory'. *Nat. Protoc.* **1**, 1306–1311 (2006).
76. Leger, M. *et al.* Object recognition test in mice. *Nat. Protoc.* **8**, 2531–2537 (2013).
77. Vorhees, C. V. & Williams, M. T. Morris water maze: procedures for assessing spatial and related forms of learning and memory. *Nat. Protoc.* **1**, 848–858 (2006).
78. Cimadevilla, J. M., Kaminsky, Y., Fenton, A. & Bures, J. Passive and active place avoidance as a tool of spatial memory research in rats. *J. Neurosci. Methods* **102**, 155–164 (2000).
79. Semmler, A. *et al.* An efficient method for fractionated whole rodent brain radiation. *Neurol. Res.* **35**, 355–359 (2013).
80. Pellow, S., Chopin, P., File, S. E. & Briley, M. Validation of open:closed arm entries in an elevated plus-maze as a measure of anxiety in the rat. *J. Neurosci. Methods* **14**, 149–167 (1985).

81. Walf, A. A. & Frye, C. A. The use of the elevated plus maze as an assay of anxiety-related behavior in rodents. *Nat. Protoc.* **2**, 322–328 (2007).
82. Schneider, C. A., Rasband, W. S. & Eliceiri, K. W. NIH Image to ImageJ: 25 years of image analysis. *Nat. Methods* **9**, 671–675 (2012).
83. Corroyer-Dulmont, A. *et al.* Detection of glioblastoma response to temozolomide combined with bevacizumab based on µMRI and µPET imaging reveals [18F]-fluoro-l-thymidine as an early and robust predictive marker for treatment efficacy. *Neuro-Oncol.* **15**, 41–56 (2013).
84. Shattuck, D. W. & Leahy, R. M. BrainSuite: an automated cortical surface identification tool. *Med. Image Anal.* **6**, 129–142 (2002).
85. Bécam, J. *et al.* Physical Activity Attenuates Brain Irradiation-Associated Skeletal Muscle Damage in the Rat. *Int. J. Radiat. Oncol. Biol. Phys.* **118**, 1081–1093 (2024).
86. Avants, B. B. *et al.* A reproducible evaluation of ANTs similarity metric performance in brain image registration. *NeuroImage* **54**, 2033–2044 (2011).

Figure 1| Experimental design. Timeline illustration of the 6-month study protocol (D: day; W: week; M: month) and the corresponding phases of adverse effects of brain irradiation, mimicking the temporal evolution of symptoms in humans (acute; early delayed; late delayed). Each rat was subjected to a fractioned whole-brain (WBI) or hemispheric-brain irradiation (HBI) on 3 consecutive days for a total dose of 30 Gy. Then, behavioral tests (PA: passive avoidance; NOR: novel object recognition; MWM: Morris water maze; EPM: elevated plus maze; OF: open field) and MRI (magnetic resonance imaging: T2-weighted imaging -T2w; diffusion tensor imaging - DTI, dynamic contrast enhancement imaging – DCE-MRI from T1-weighted imaging with gadolinium contrast agent) sessions were performed. The behavioral tests and MRI were sequentially realized at different times after brain irradiation (from 1 week up to 6 months). The different behavioral tests and MRI acquisitions were performed in the order mentioned from bottom to top of the figure. At 2 h after the last irradiation or at the end of experimental protocol, the brains were harvested and processed for immunohistochemistry analyses (IHC).

Figure 2| Dose-volume histograms and irradiation-induced acute DNA damage. Dose-volume histograms (DVH) and dose deposition maps were generated using a treatment planning system (TPS) in hemispheric and whole-brain irradiation groups (HBI and WBI, respectively) following a 10 Gy fraction. **(a)** DVH obtained in the right hemisphere (irradiated hemisphere in the 2 groups). Inset: dose deposition maps and D50 values delivered to striatum, hippocampus and cortex. **(b - c**) Irradiation-induced DNA damage was evaluated 2 hours after the end of the irradiation after WBI or HBI by immunostaining of γ-H2AX protein (red), a specific marker of DNA double-strand breaks. Representative images of γ-H2AX foci in the cortex of CTL, HBI and WBI animals: **(b)** in the left hemisphere and **(c)** in the right hemisphere. In HBI rats, only the right hemisphere received irradiation. Cell nuclei were stained with Hoechst 33342 (blue). Images were acquired under x20 magnification (scale bar = 100 µm) and zoom inserts were added (scale bar = 100 µm).

Figure 3| Body weight follow-up and survival rate. (a) Evolution of mean body weight over time in each experimental group after brain irradiation: non-irradiated rats (CTL: full line, n=16), rats submitted to right hemispheric brain irradiation (HBI: dot line, n=14) or whole-brain irradiation (WBI: dash line, n=10-12). Mean + SD; two-way ANOVA followed by Fisher's LSD test: * $p < 0.05$, *** $p < 0.001$, **** $p < 0.0001$ for WBI vs CTL or HBI. **(b)** Impact of brain irradiation on survival in each experimental group: non-irradiated rats (CTL: full line, n=16), rats submitted to right hemispheric brain irradiation (HBI: dot line, n=14) or whole-brain irradiation (WBI: dash line, n=12). From Kaplan-Meier curves, the statistical analyses were based on a log-rank test.

Figure 4| Learning and memory performances. (a) Spatial learning was evaluated using the Morris water maze. The distance moved by the animals in the pool before finding the hidden platform was quantified. **(b)** For reference memory based on Morris water maze, the cumulative duration in the target quadrant during the probe test was measured. Non-irradiated

control rats (CTL: white, n=15-16), rats submitted to right hemispheric brain irradiation (HBI: gray, n=13-14) or whole-brain irradiation (WBI: black, n=10-11). **(c)** From the novel object recognition test, the working memory was evaluated by assessing the recognition index: non-irradiated rats (CTL: white, n=11-15), rats submitted to right hemispheric brain irradiation (HBI: gray, n=7-14) or whole-brain irradiation (WBI: black, n=9-11). **(d)** Using the passive avoidance test, long-term memory was estimated by the latency for the rats to enter the small dark compartment. Non-irradiated rats (CTL: white, n=9), rats submitted to right hemispheric brain irradiation (HBI: gray, n=11) or whole-brain irradiation (WBI: black, n=10). The times of the experiments are represented as W = week and M = month. Mean + SD; two-way ANOVA followed by Fisher's LSD test: * $p < 0.05$, ** $p < 0.01$, **** $p < 0.0001$.

Figure 5| Locomotor and anxiety-like behaviors. (a) The anxiety-like behavior was evaluated by the total time spent by the rat in the center and in the periphery of the open field. The total distance moved was measured to study the locomotor abilities of animals. **(b)** The anxiety-like behavior of the animals was evaluated by the time spent by the rats in the center, open arms and closed arms of the elevated plus maze apparatus. The tasks were performed at 6 months post-irradiation (M6). Non-irradiated rats (CTL: white, n=4), rats submitted to right hemispheric brain irradiation (HBI: gray, n=5) or whole-brain irradiation (WBI: black, n=9). Mean + SD; one-way ANOVA followed by Fisher's LSD test: * $p < 0.05$, ** $p < 0.01$, *** $p < 0.001$.

Figure 6| MRI analyses of brain macrostructure and vasculature. (a) Representative T2-weighted images acquired at 6 months in non-irradiated group (CTL), hemispheric brain irradiation (HBI) or whole-brain irradiation (WBI). **(b)** From these anatomical images, the whole brain volume was quantified in control group (CTL: white, n=9), and after hemispheric brain irradiation (HBI: gray, n=11) or whole-brain irradiation (WBI: black, n=10). Mean + SD; one-way ANOVA followed by Fisher's LSD test: * $p < 0.05$. **(c)** Quantitative values of cerebral blood volume (CBV) at 6 months post-irradiation in the right hemisphere and left hemisphere in 5

regions of interest (*i.e.* cortex, hippocampus, corpus callosum, striatum and thalamus) in non-irradiated rats (CTL: white, n=9), rats submitted to right hemispheric brain irradiation (HBI: gray, n=11) or whole-brain irradiation (WBI: black, n=10). Mean + SD; one-way ANOVA followed by Fisher's LSD test: * $p < 0.05$, ** $p < 0.01$.

Figure 7| Evaluation of blood-brain barrier permeabilization by dynamic contrast enhancement imaging (DCE-MRI). (a) Representative T1-weighted images acquired after intravenous injection of gadolinium. The images were obtained at 6 months in non-irradiated group (CTL), hemispheric brain irradiation (HBI) or whole-brain irradiation (WBI). **b-d,** Time-course curves of T1-weighted signal were extracted **(b)** in the cortex, **(c)** the hippocampus and **(d)** the temporal muscles. The T1 signal enhancement for each animal was quantified by a normalization of the signal relative to the images acquired before gadolinium administration. Non-irradiated rats (CTL: white, n=9), rats submitted to right hemispheric brain irradiation (HBI: gray, n=11) or whole-brain irradiation (WBI: black, n=10). Mean + SD; repeated ANOVA followed by Fisher's LSD test: * $p < 0.05$ WBI versus CTL, ££ $p<0.01$ HBI versus CTL, # $p < 0.05$ and ## $p<0.01$ WBI versus HBI.

Figure 8| Assessment of brain microstructure evolution following hemispheric or whole-brain irradiation by mean diffusivity (MD). Quantitative representation of MD values in the right hemisphere in 5 regions of interest (*i.e.* cortex, hippocampus, corpus callosum, striatum and thalamus) at 1, 3- and 6-months post-irradiation. MD values were measured for non-irradiated rats (CTL: white, n=9), rats submitted to right hemispheric brain irradiation (HBI: gray, n=10-11) or whole-brain irradiation (WBI: black, n=8-10). Mean + SD, two-way ANOVA followed by Fisher's LSD test: * $p < 0.05$, ** $p < 0.01$, *** $p < 0.001$, **** $p < 0.0001$.

Figure 9| Effects of hemispheric or whole-brain irradiation on microglia activation. (a) Representative photographs of Iba1 immunostaining (microglial cells, in green) in the cortex and the hippocampus in the right hemisphere of non-irradiated (CTL group), only right

hemisphere irradiated (HBI group) and whole-brain irradiated (WBI) rats**. b-c,** Quantification of the total area marked by Iba1 positive cells relative to total area of images and number of positive cells is shown as histograms in **(b)** the cortex and **(c)** the hippocampus. **(d)** CD68 immunoreactivity revealing microglia activation: representative photographs of the CD68 immunostaining (macrophages cells, in red) in the cortex and the hippocampus in the right hemisphere of non-irradiated (CTL group), only right hemisphere irradiated (HBI group) and whole-brain irradiated (WBI) rats. **e-f,** Quantification of the total area marked by CD68 positive cells relative to total area of images and number of positive cells is shown as histograms in **(e)** the cortex and **(f)** the hippocampus. All images were acquired under x 20 magnification (n=3 rats for each experimental group; scale bar = 200 µm; insert scale bar = 50 µm). Mean + SD, one-way ANOVA followed by Fisher's LSD test: * $p < 0.05$, ** $p < 0.01$.

Figure 10| Effects of hemispheric or whole-brain irradiation on astrogliosis and white matter. (a) GFAP immunoreactivity of reactive astrocytes: **r**epresentative photographs of GFAP immunostaining (astrocytes, in green) in the cortex and the hippocampus in the right hemisphere of non-irradiated (CTL group), only right hemisphere irradiated (HBI group) and whole-brain irradiated (WBI) rats**. b-c,** Quantification of the total area marked by GFAP positive cells relative to total area of images and number of positive cells is shown as histograms in **(b)** the cortex and **(c)** the hippocampus. Images were acquired under x 20 magnification (n=3 rats for each experimental group; scale bar = 200 µm; insert scale bar = 50 µm). **(d)** Myelin PLP immunoreactivity of white matter: **r**epresentative photographs of the PLP immunostaining (myelin of white matter, in red) of the striatum in the right hemisphere of non-irradiated (CTL group), only right hemisphere irradiated (HBI group) and whole-brain irradiated (WBI) rats. **(e)** Quantification of the total area marked by PLP positive cells relative to total area of images is shown. Images were acquired under x 10 magnification (n=3 rats for each experimental group; scale bar = 200 µm; insert scale bar = 50 µm). Mean + SD, one-way ANOVA followed by Fisher's LSD test: * $p < 0.05$, ** $p < 0.01$, ** $p < 0.001$, ** $p < 0.0001$.

Figure 11| Effects of hemispheric or whole-brain irradiation on mature neurons and neural stem cells. (a) NeuN immunoreactivity of neurons: representative photographs of NeuN immunostaining (mature neurons cells, in green) in the cortex and the hippocampus in the right hemisphere of non-irradiated (CTL group), only right hemisphere irradiated (HBI group) and whole-brain irradiated (WBI) rats. **(b)** Sox2 immunoreactivity revealing neural stem cells (NSC): representative photographs of the Sox2 immunostaining (NSC, in red) in the cortex and the hippocampus in the right hemisphere of non-irradiated (CTL group), only right hemisphere irradiated (HBI group) and whole-brain irradiated (WBI) rats. **c-d,** Quantification of the total area marked by **(c)** NeuN positive cells or **(d)** Sox2 positive cells relative to total area of images and number of positive cells in the cortex. **e-f,** Quantification of the total area marked by **(e)** NeuN positive cells or **(f)** Sox2 positive cells relative to total area of images and number of positive cells in the hippocampus. All images were acquired under x 20 magnification (n=3 rats for each experimental group; scale bar = 200 µm; insert scale bar = 50 µm). Mean + SD, one-way ANOVA followed by Fisher's LSD test: * $p < 0.05$, ** $p < 0.01$.

Figure 12: Effects of hemispheric or whole-brain irradiation on vessels and BBB integrity. a-b, Representative photographs of RECA-1 (endothelial cells, in green) and ZO-1 (tight junctions, in red) immunostainings and merged images (RECA-1/ZO-1 superposition, in yellow) in **(a)** the cortex and **(b)** the hippocampus in the right hemisphere of non-irradiated (CTL group), only right hemisphere irradiated (HBI group) and whole-brain irradiated (WBI) rats. **c-d,** Quantification of the positive area marked by RECA-1 relative to total area of images corresponding to vessel area, the positive area marked by ZO-1 relative to total area of images corresponding to tight junction area and the positive ZO-1 staining in vessels. Quantifications are presented as histograms in **(c)** the cortex and **(d)** the hippocampus. All images were acquired under x 10 magnification (n=3 rats for each experimental group; scale bar = 200 µm; insert scale bar = 50 µm). Mean + SD, one-way ANOVA followed by Fisher's LSD test: * $p < 0.05$, ** $p < 0.01$.

Figure 1

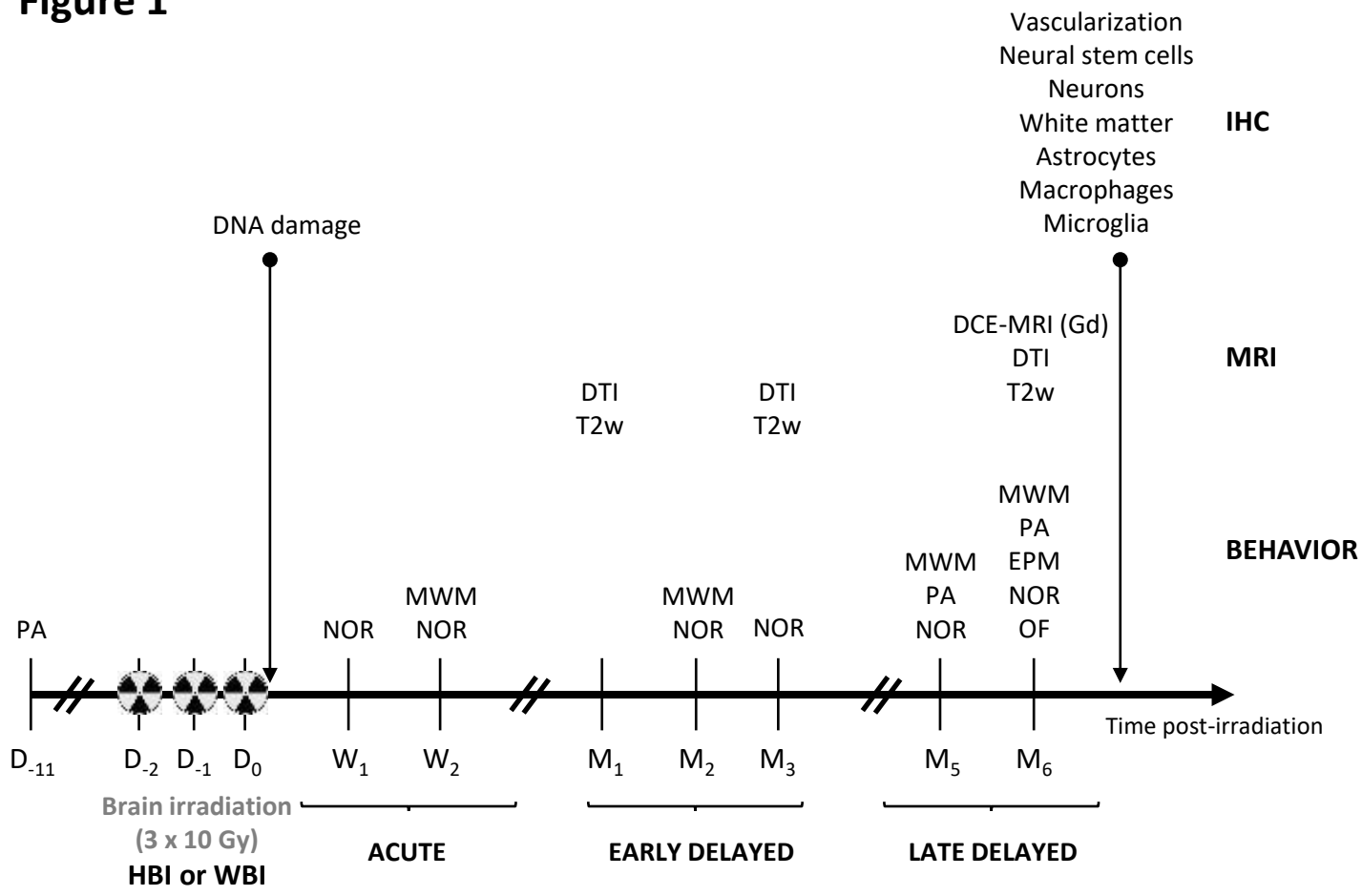
Vascularization
Neural stem cells
Neurons
White matter
Astrocytes
Macrophages
Microglia
IHC
DNA damage
DCE-MRI (Gd)
DTI
T2w
MRI
DTI
T2w
DTI
T2w
MWM
PA
EPM
NOR
OF
BEHAVIOR
MWM
PA
NOR
MWM
NOR
NOR
MWM
NOR
PA
Time post-irradiation
D-11
D-2
D-1
D0
W1
W2
M1
M2
M3
M5
M6
Brain irradiation
(3 x 10 Gy)
HBI or WBI
ACUTE
EARLY DELAYED
LATE DELAYED

Figure 2

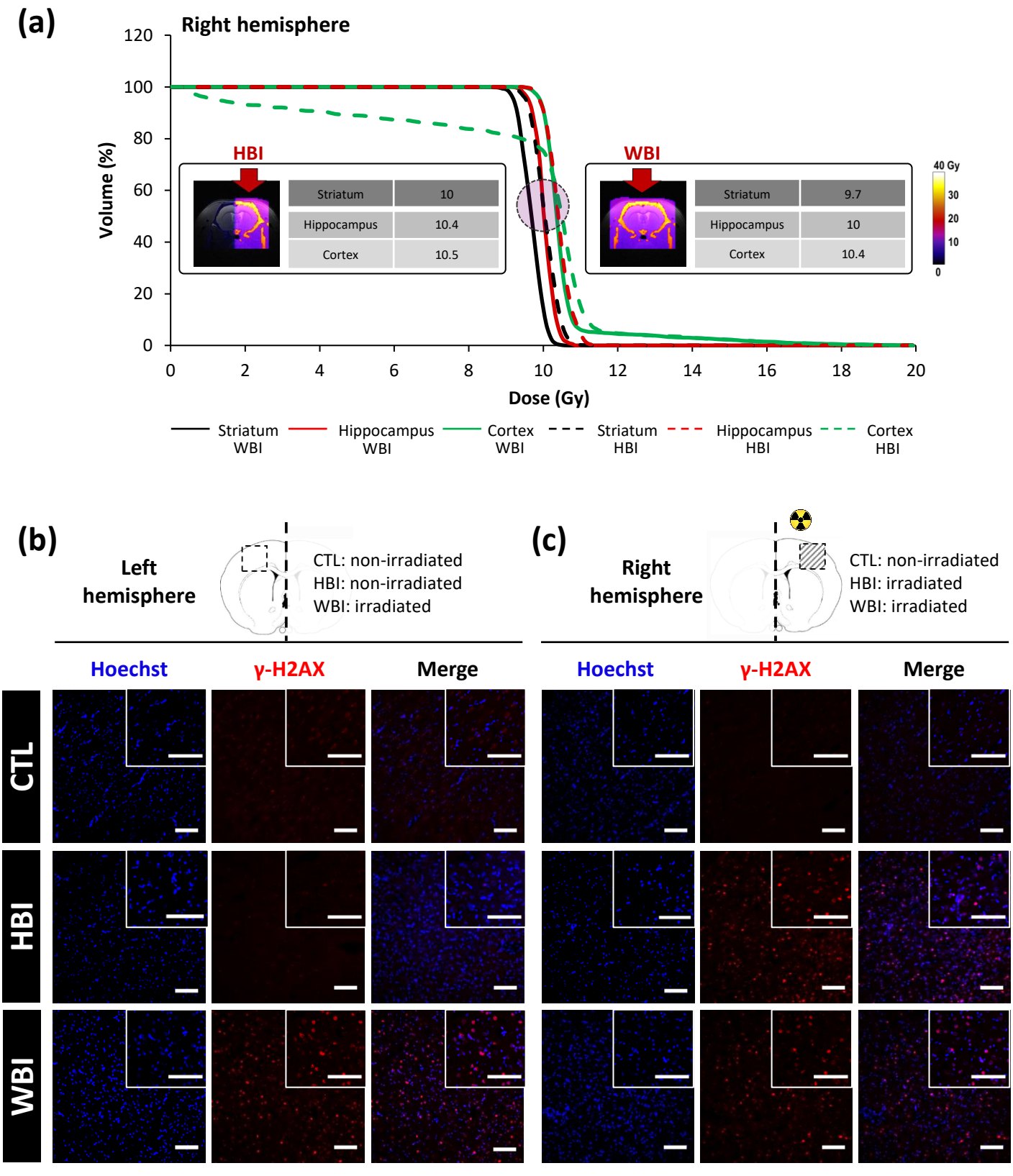
(a)
Right hemisphere
Volume (%)
Dose (Gy)
HBI
WBI
Striatum 10
Hippocampus 10.4
Cortex 10.5
Striatum 9.7
Hippocampus 10
Cortex 10.4
40 Gy
30
20
10
0
Striatum WBI
Hippocampus WBI
Cortex WBI
Striatum HBI
Hippocampus HBI
Cortex HBI
(b)
Left hemisphere
CTL: non-irradiated
HBI: non-irradiated
WBI: irradiated
(c)
Right hemisphere
CTL: non-irradiated
HBI: irradiated
WBI: irradiated
Hoechst
γ-H2AX
Merge
CTL
HBI
WBI

Figure 3

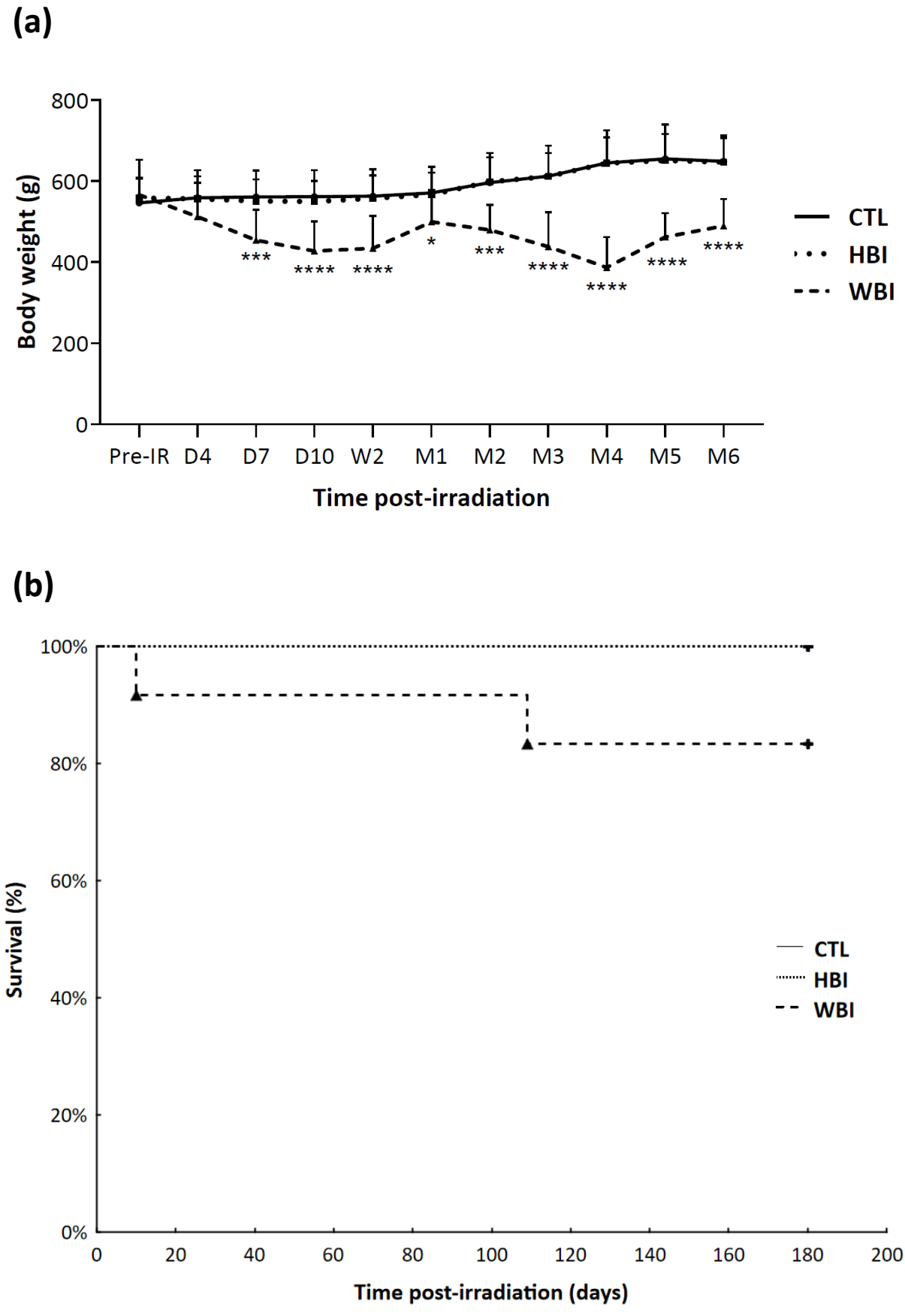
(a)
Body weight (g)
800
600
400
200
0
Pre-IR
D4
D7
D10
W2
M1
M2
M3
M4
M5
M6
Time post-irradiation
CTL
HBI
WBI
(b)
Survival (%)
100%
80%
60%
40%
20%
0%
0
20
40
60
80
100
120
140
160
180
200
Time post-irradiation (days)
CTL
HBI
WBI

Figure 4

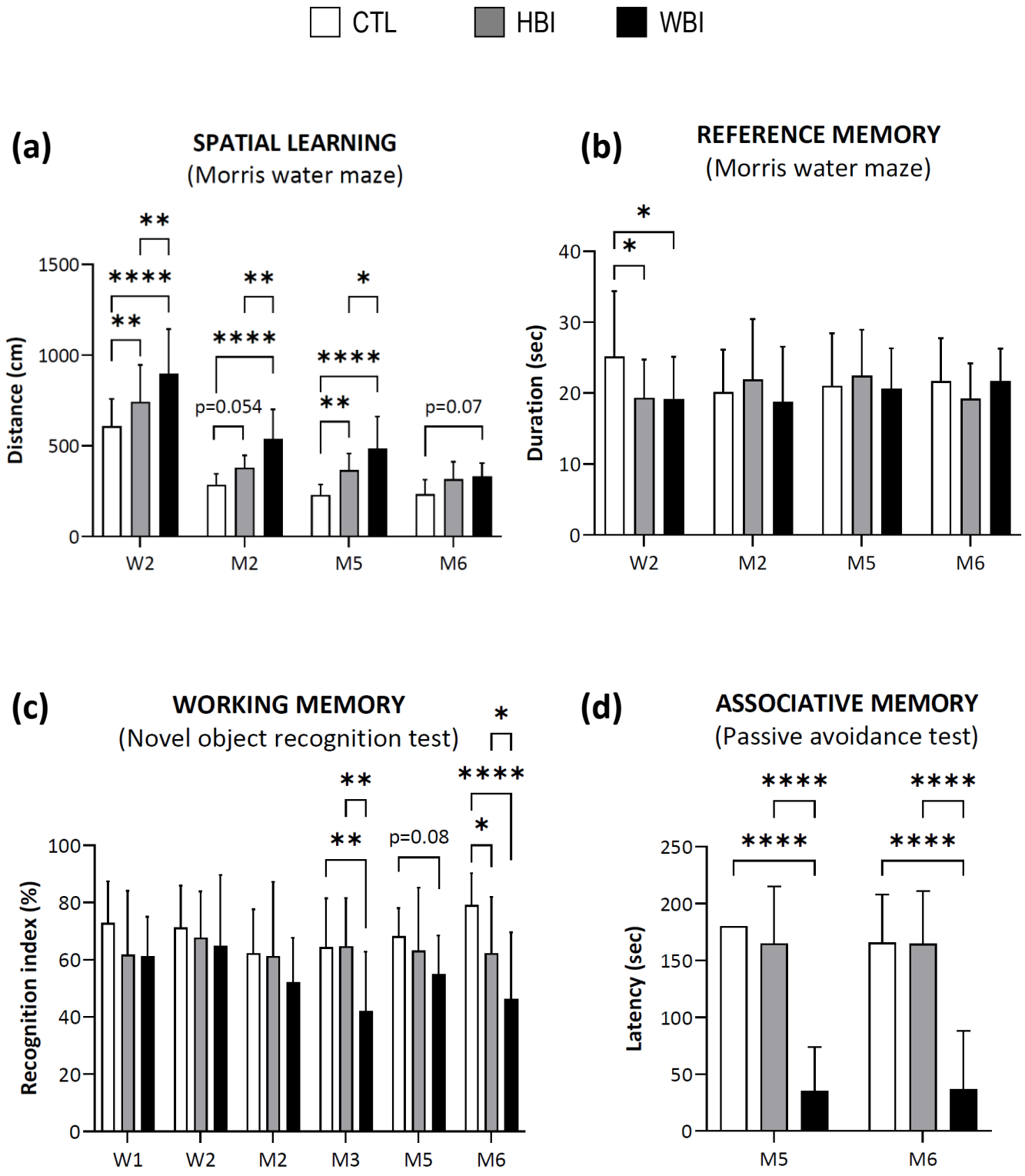
CTL
HBI
WBI
(a)
SPATIAL LEARNING
(Morris water maze)
Distance (cm)
1500
1000
500
0
W2
M2
M5
M6
p=0.054
p=0.07
(b)
REFERENCE MEMORY
(Morris water maze)
Duration (sec)
40
30
20
10
0
W2
M2
M5
M6
(c)
WORKING MEMORY
(Novel object recognition test)
Recognition index (%)
100
80
60
40
20
0
W1
W2
M2
M3
M5
M6
p=0.08
(d)
ASSOCIATIVE MEMORY
(Passive avoidance test)
Latency (sec)
250
200
150
100
50
0
M5
M6

Figure 5

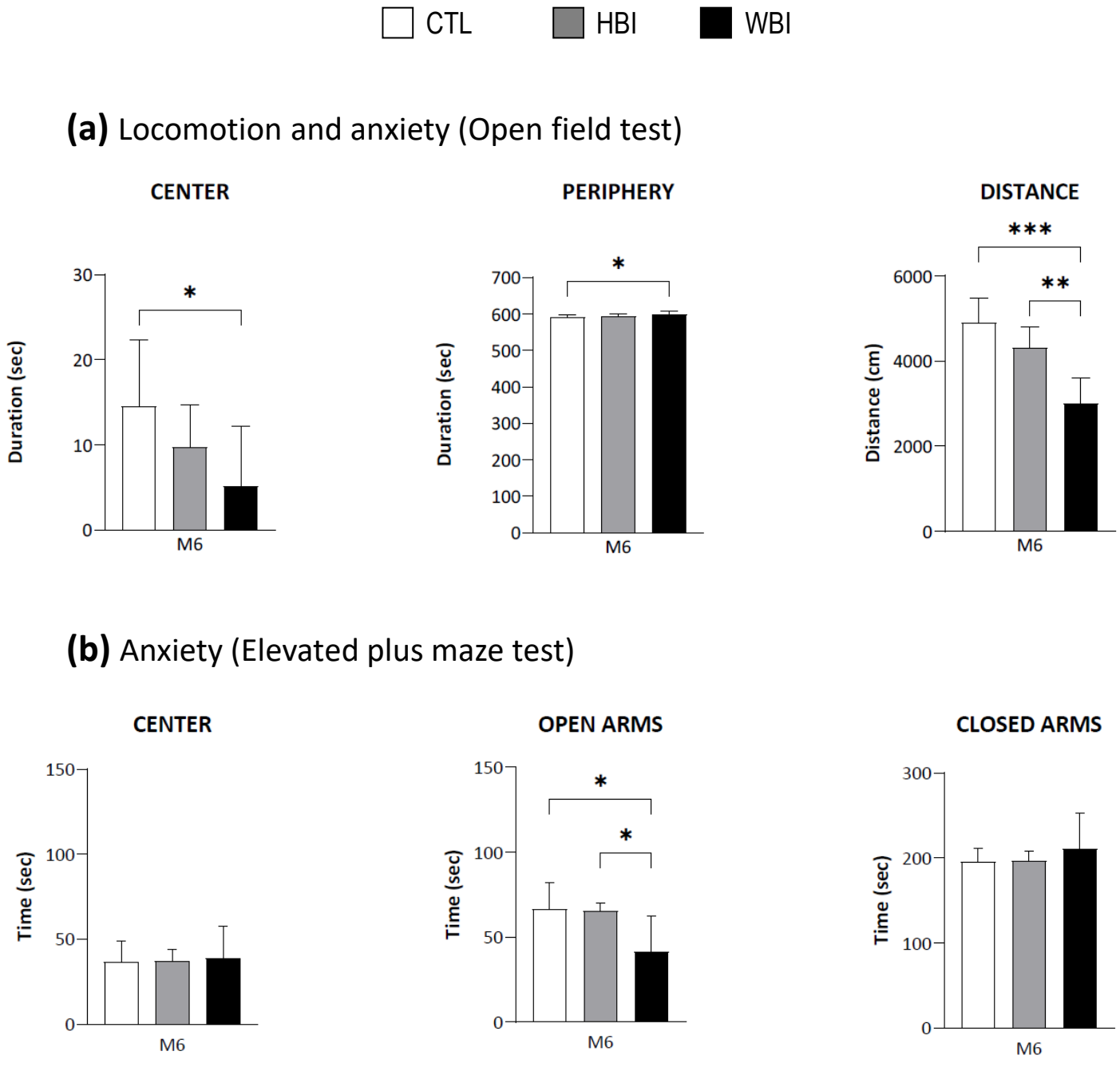
CTL
HBI
WBI
(a) Locomotion and anxiety (Open field test)
CENTER
Duration (sec)
30
20
10
0
*
M6
PERIPHERY
Duration (sec)
700
600
500
400
300
200
100
0
*
M6
DISTANCE
Distance (cm)
6000
4000
2000
0
***
**
M6
(b) Anxiety (Elevated plus maze test)
CENTER
Time (sec)
150
100
50
0
M6
OPEN ARMS
Time (sec)
150
100
50
0
*
*
M6
CLOSED ARMS
Time (sec)
300
200
100
0
M6

Figure 6

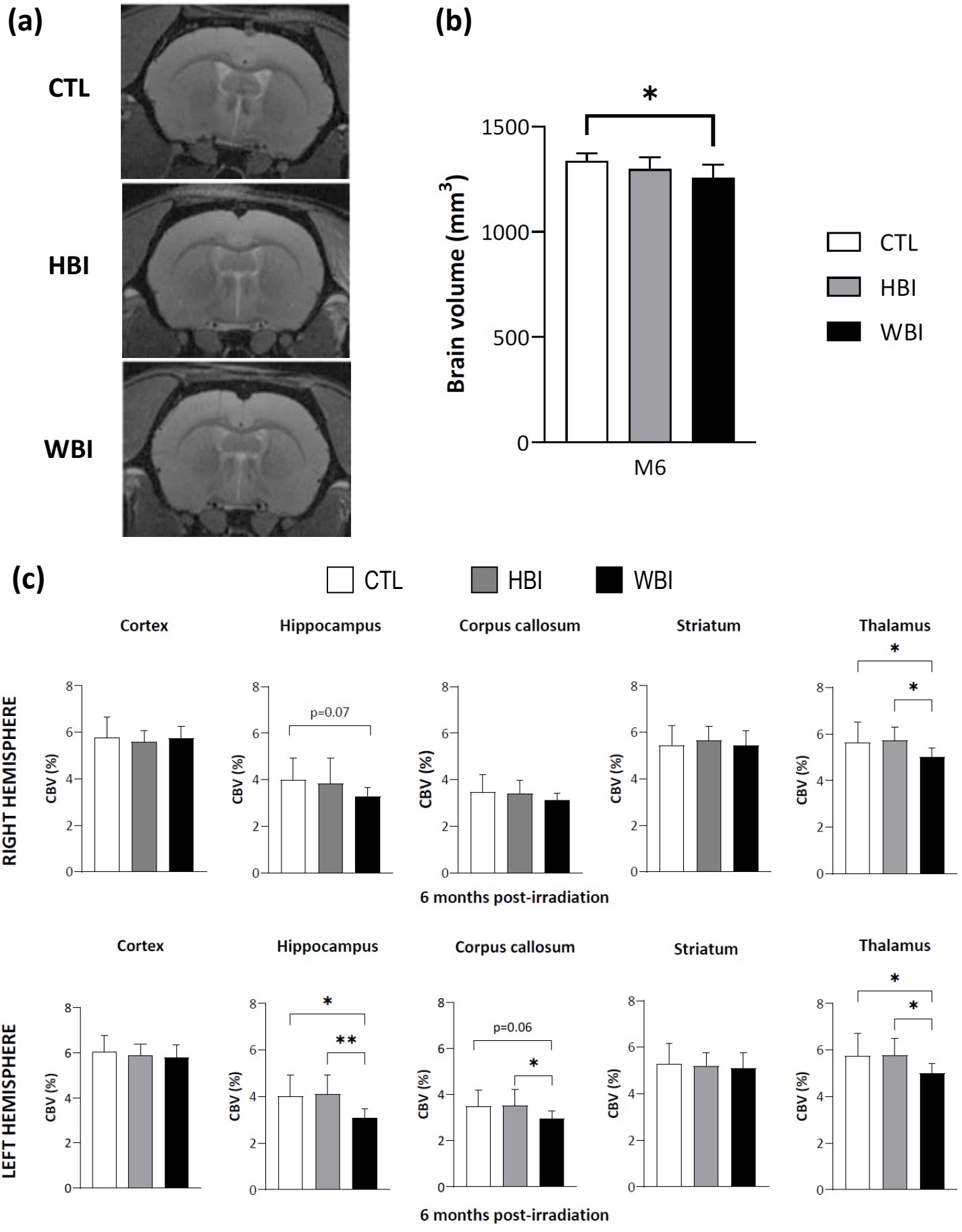
(a)
CTL
HBI
WBI
(b)
*
1500
1000
500
0
Brain volume (mm3)
M6
CTL
HBI
WBI
(c)
CTL
HBI
WBI
Cortex
Hippocampus
Corpus callosum
Striatum
Thalamus
RIGHT HEMISPHERE
CBV (%)
p=0.07
*
6 months post-irradiation
LEFT HEMISPHERE
p=0.06
**

Figure 7

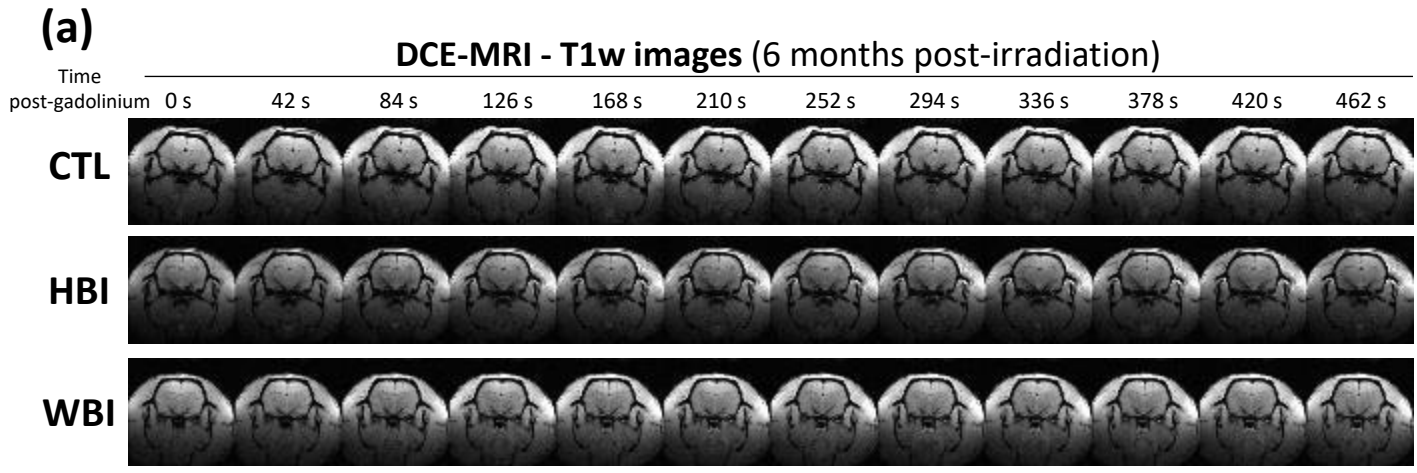
(a)
DCE-MRI - T1w images (6 months post-irradiation)
Time post-gadolinium
0 s
42 s
84 s
126 s
168 s
210 s
252 s
294 s
336 s
378 s
420 s
462 s
CTL
HBI
WBI

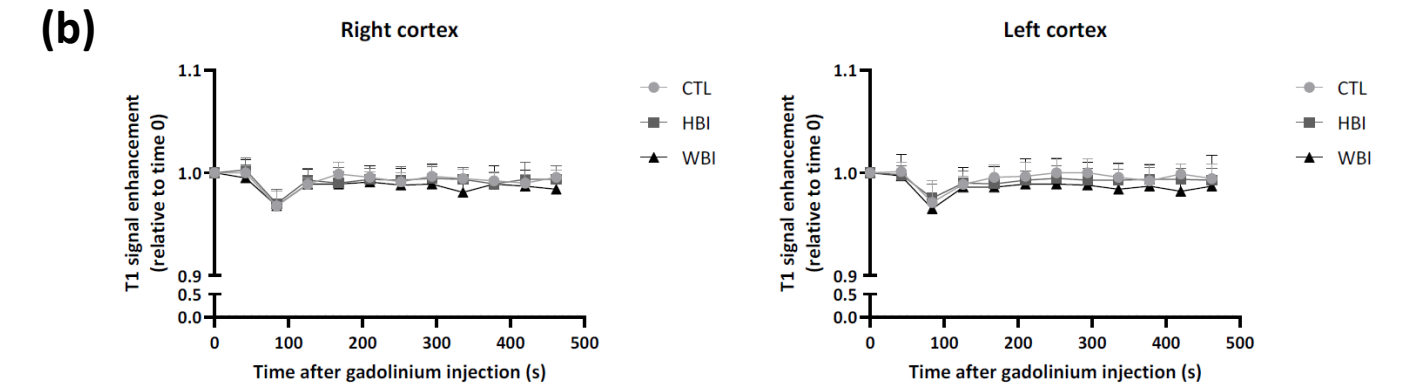
(b)
Right cortex
Left cortex
T1 signal enhancement (relative to time 0)
Time after gadolinium injection (s)
CTL
HBI
WBI

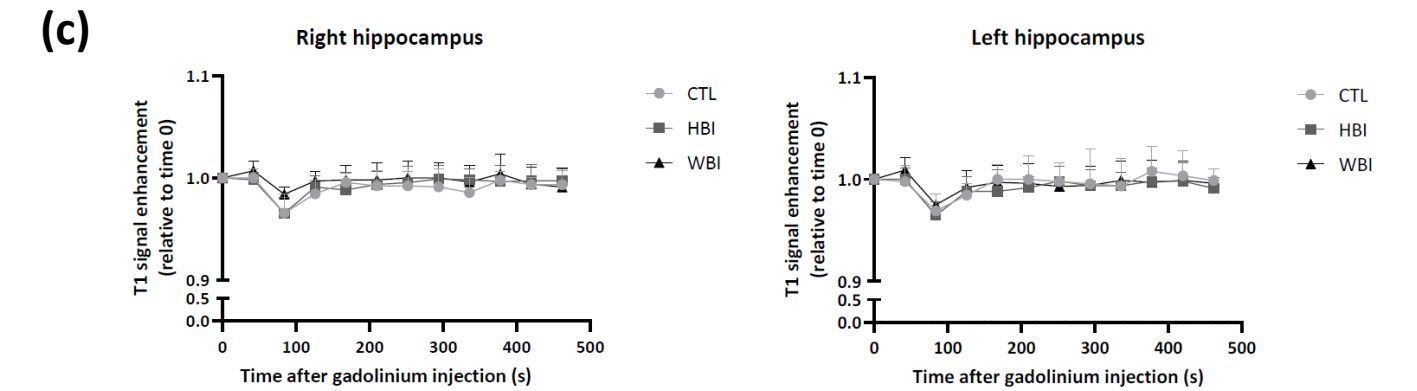
(c)
Right hippocampus
Left hippocampus
T1 signal enhancement (relative to time 0)
Time after gadolinium injection (s)
CTL
HBI
WBI

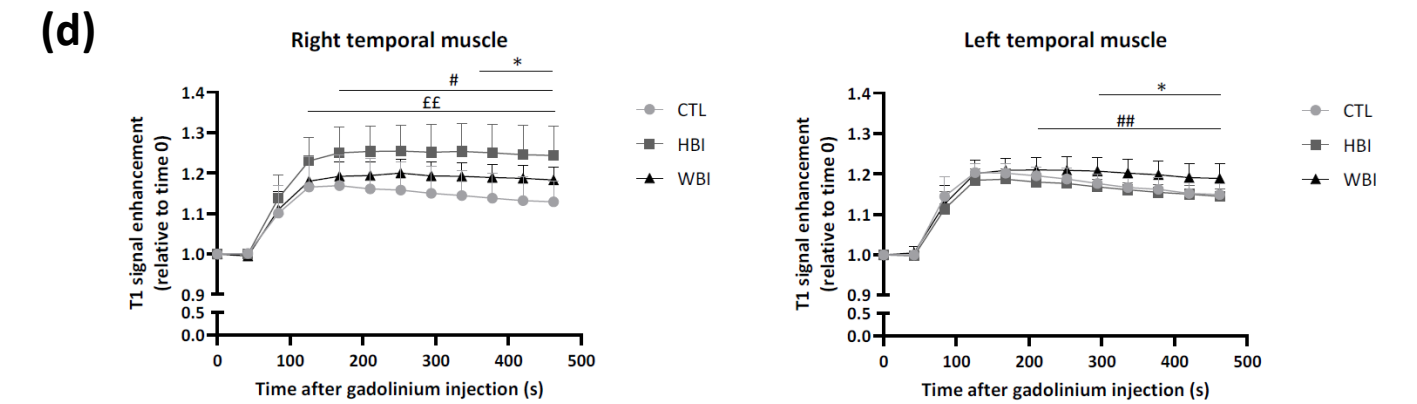
(d)
Right temporal muscle
Left temporal muscle
#
*
££
##
T1 signal enhancement (relative to time 0)
Time after gadolinium injection (s)
CTL
HBI
WBI

Figure 8

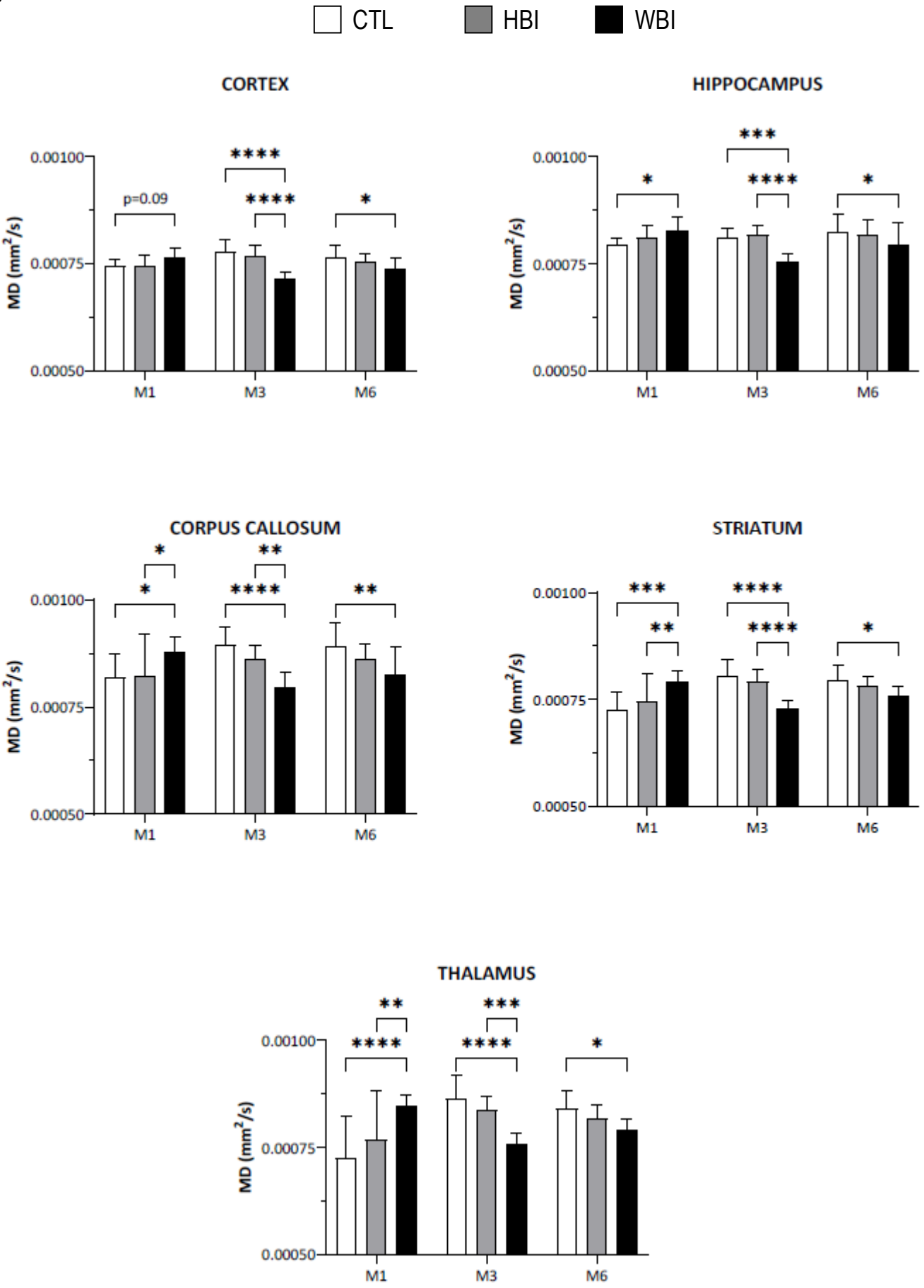
CTL
HBI
WBI
CORTEX
HIPPOCAMPUS
CORPUS CALLOSUM
STRIATUM
THALAMUS
MD (mm²/s)
0.00100
0.00075
0.00050
M1
M3
M6
p=0.09
*
**
***
****

Figure 9

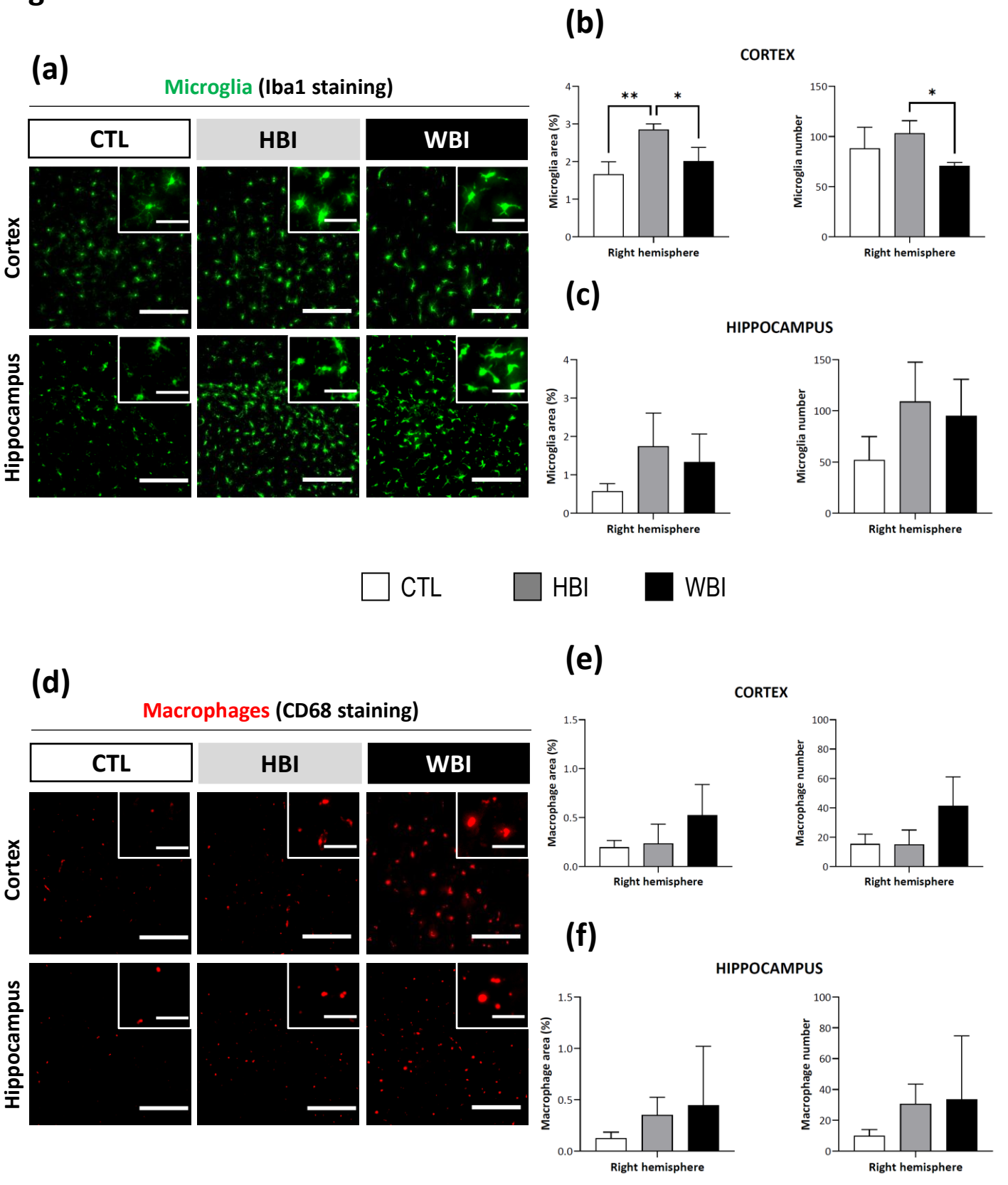
(a)
Microglia (Iba1 staining)
CTL
HBI
WBI
Cortex
Hippocampus
(b)
CORTEX
Microglia area (%)
Microglia number
Right hemisphere
**
*
(c)
HIPPOCAMPUS
Microglia area (%)
Microglia number
Right hemisphere
CTL
HBI
WBI
(d)
Macrophages (CD68 staining)
CTL
HBI
WBI
Cortex
Hippocampus
(e)
CORTEX
Macrophage area (%)
Macrophage number
Right hemisphere
(f)
HIPPOCAMPUS
Macrophage area (%)
Macrophage number
Right hemisphere

Figure 10

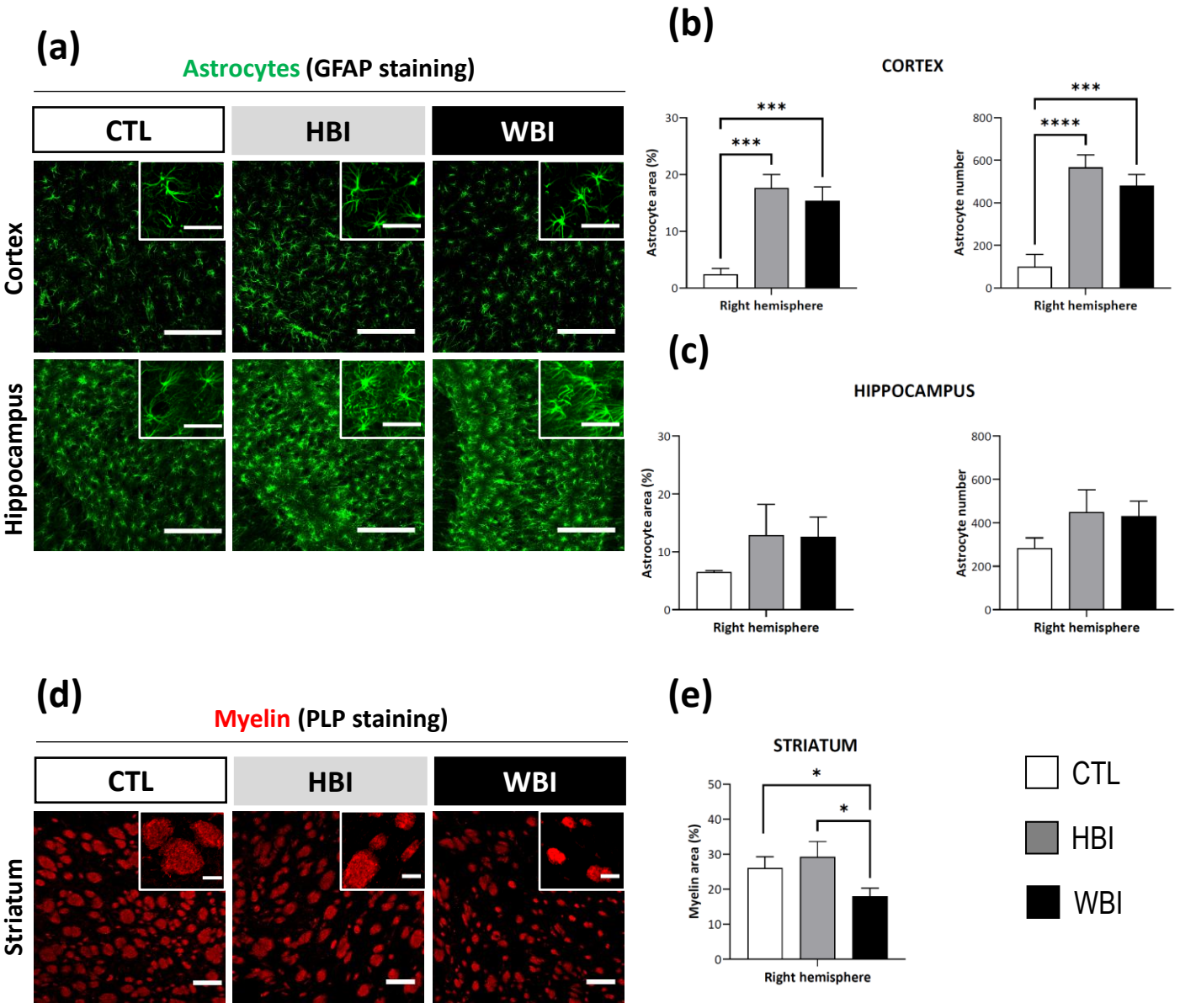
(a)
Astrocytes (GFAP staining)
CTL
HBI
WBI
Cortex
Hippocampus
(b)
CORTEX
Astrocyte area (%)
Astrocyte number
Right hemisphere
***
****
(c)
HIPPOCAMPUS
Astrocyte area (%)
Astrocyte number
Right hemisphere
(d)
Myelin (PLP staining)
CTL
HBI
WBI
Striatum
(e)
STRIATUM
Myelin area (%)
Right hemisphere
*
CTL
HBI
WBI

Figure 11

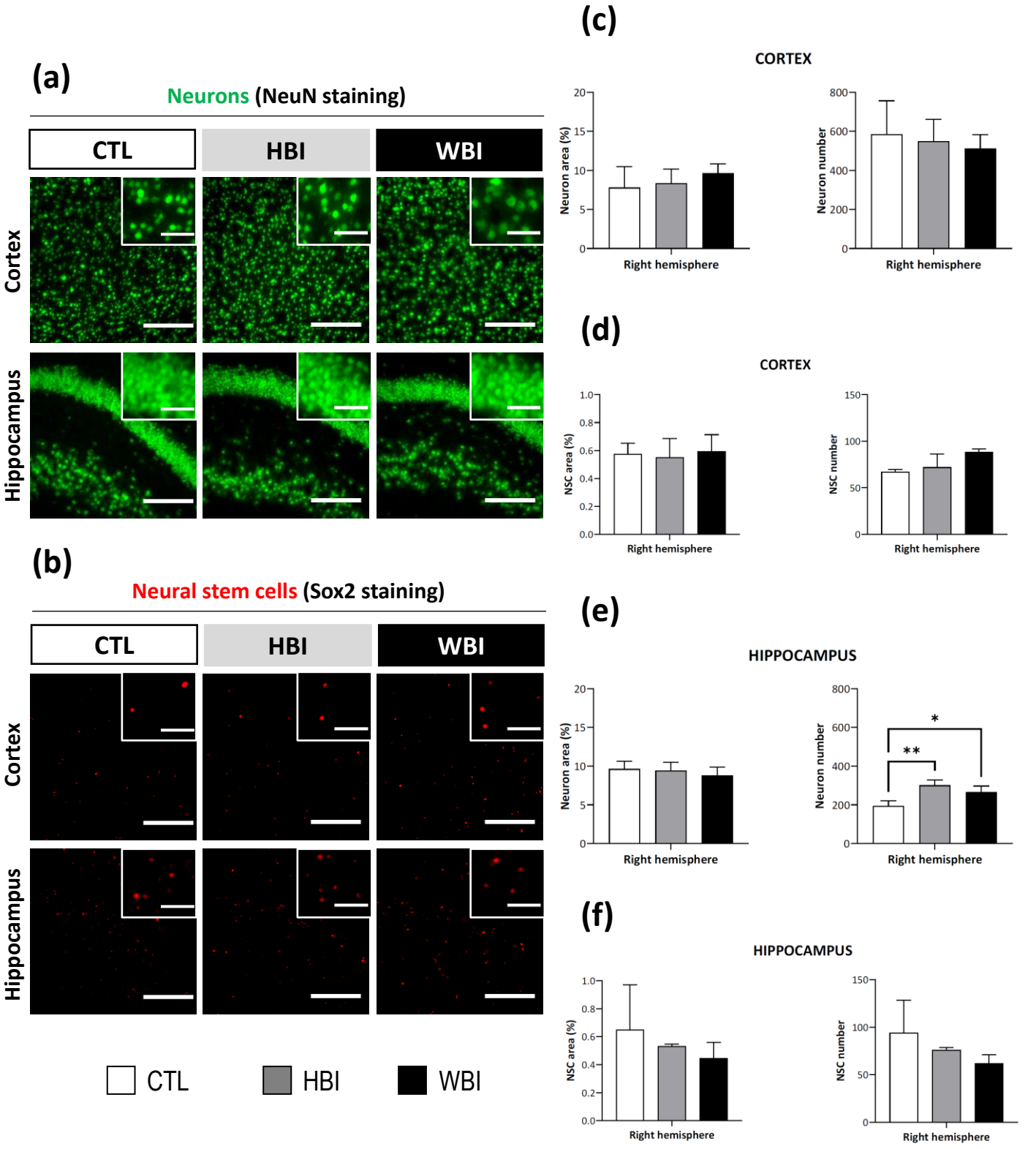
(a)
Neurons (NeuN staining)
CTL
HBI
WBI
Cortex
Hippocampus
(b)
Neural stem cells (Sox2 staining)
CTL
HBI
WBI
Cortex
Hippocampus
CTL
HBI
WBI
(c)
CORTEX
Neuron area (%)
Right hemisphere
Neuron number
Right hemisphere
(d)
CORTEX
NSC area (%)
Right hemisphere
NSC number
Right hemisphere
(e)
HIPPOCAMPUS
Neuron area (%)
Right hemisphere
Neuron number
*
**
Right hemisphere
(f)
HIPPOCAMPUS
NSC area (%)
Right hemisphere
NSC number
Right hemisphere

Figure 12

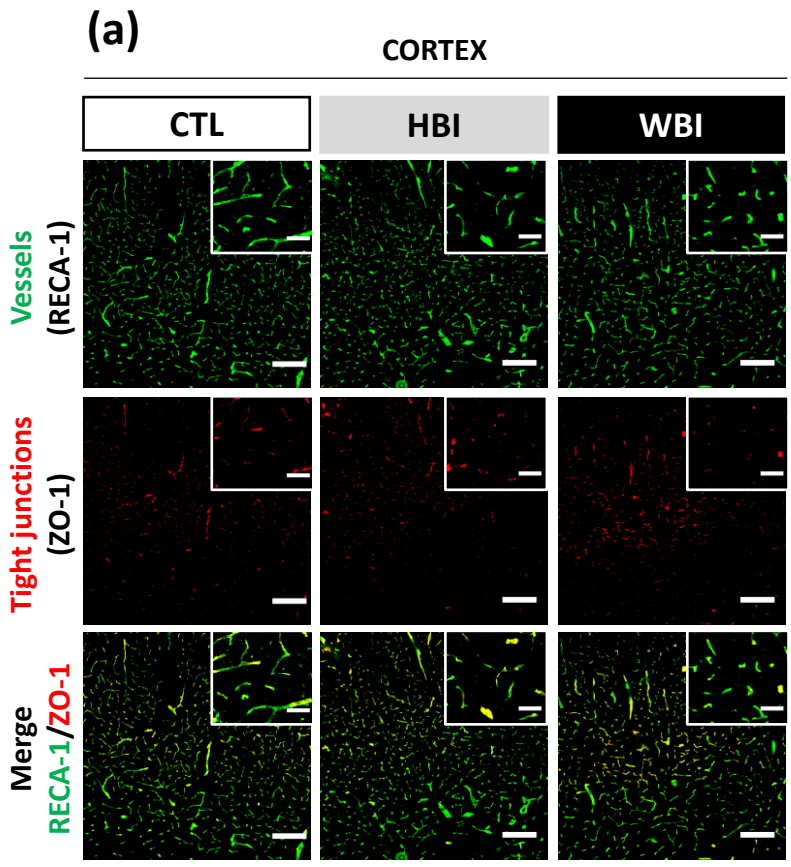
(a)
CORTEX
CTL
HBI
WBI
Vessels (RECA-1)
Tight junctions (ZO-1)
Merge RECA-1/ZO-1

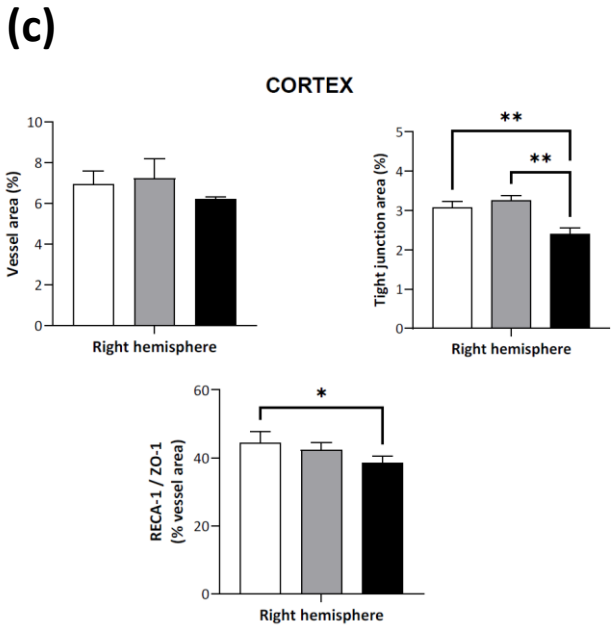
(c)
CORTEX
Vessel area (%)
Right hemisphere
Tight junction area (%)
**
**
RECA-1 / ZO-1 (% vessel area)
*
Right hemisphere


CTL
HBI
WBI

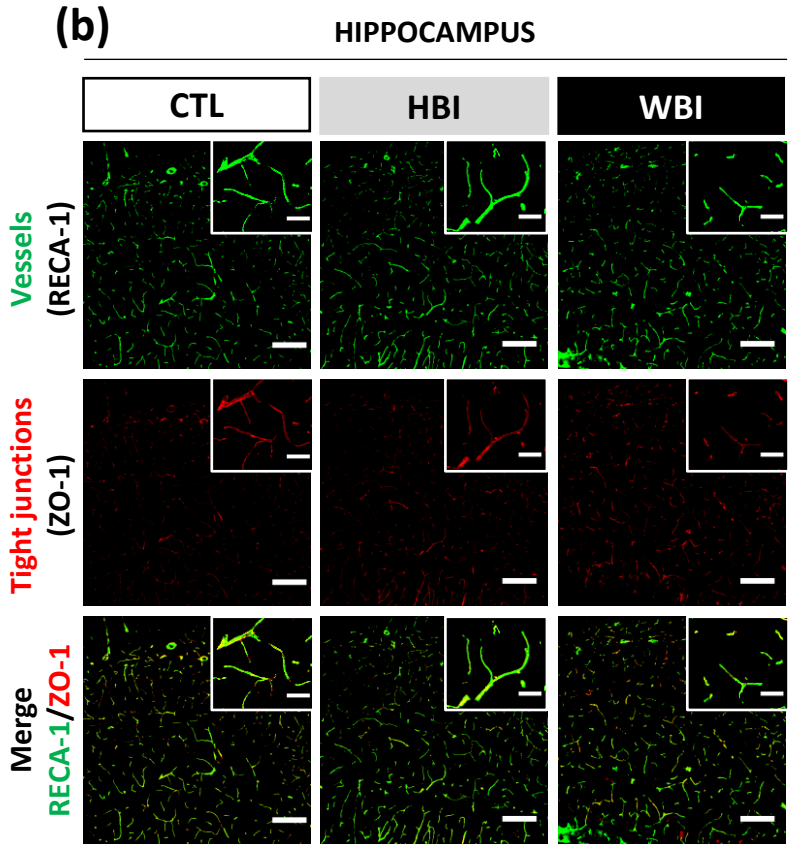
(b)
HIPPOCAMPUS
CTL
HBI
WBI
Vessels (RECA-1)
Tight junctions (ZO-1)
Merge RECA-1/ZO-1

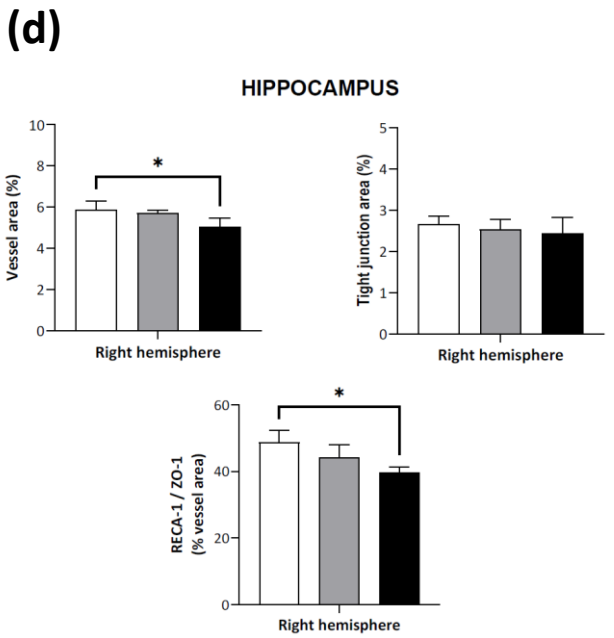
(d)
HIPPOCAMPUS
Vessel area (%)
*
Right hemisphere
Tight junction area (%)
Right hemisphere
RECA-1 / ZO-1 (% vessel area)
*
Right hemisphere

Supplementary Figure 1

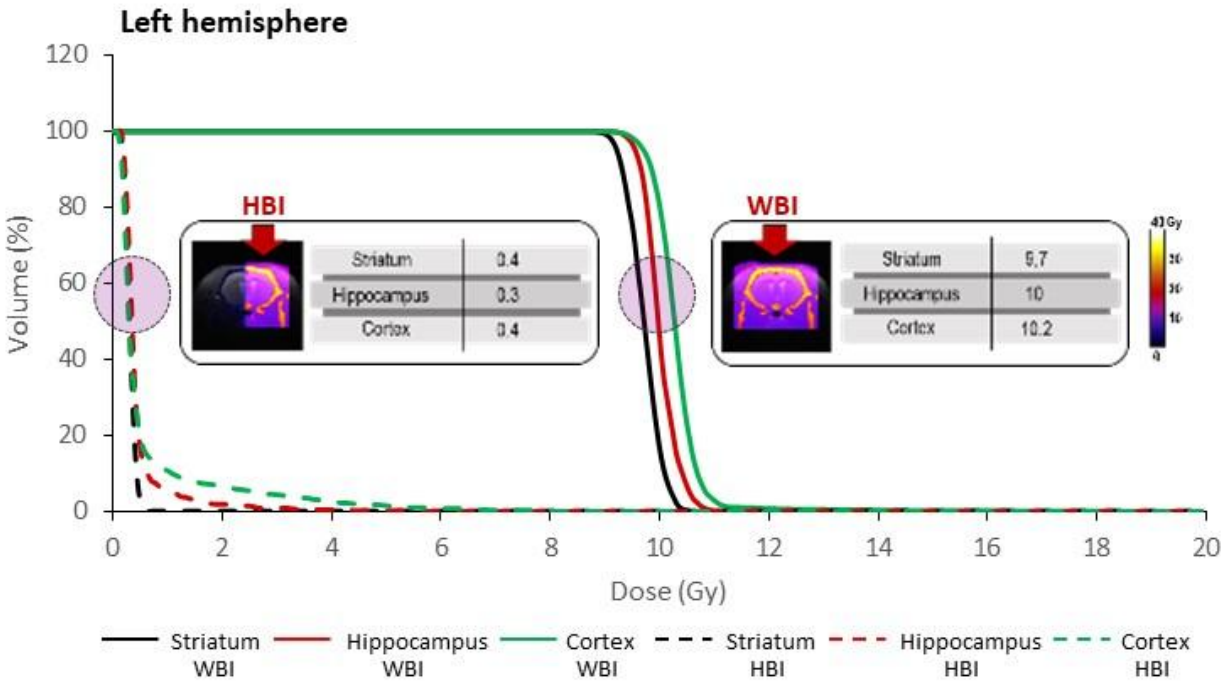

<u>Supplementary Figure 1</u>: Dosimetry analyses in the left hemisphere. Dose-volume histograms (DVH) and dose deposition maps were generated through the use of a treatment planning system (TPS) in hemispheric and whole-brain irradiation groups (HBI and WBI, respectively) following a 10 Gy fraction. DVH obtained in the left hemisphere (irradiated hemisphere for WBI group and nonirradiated hemisphere for HBI group). Inset: dose deposition maps and D50 values delivered to the striatum, the hippocampus and the cortex.

Supplementary Figure 2

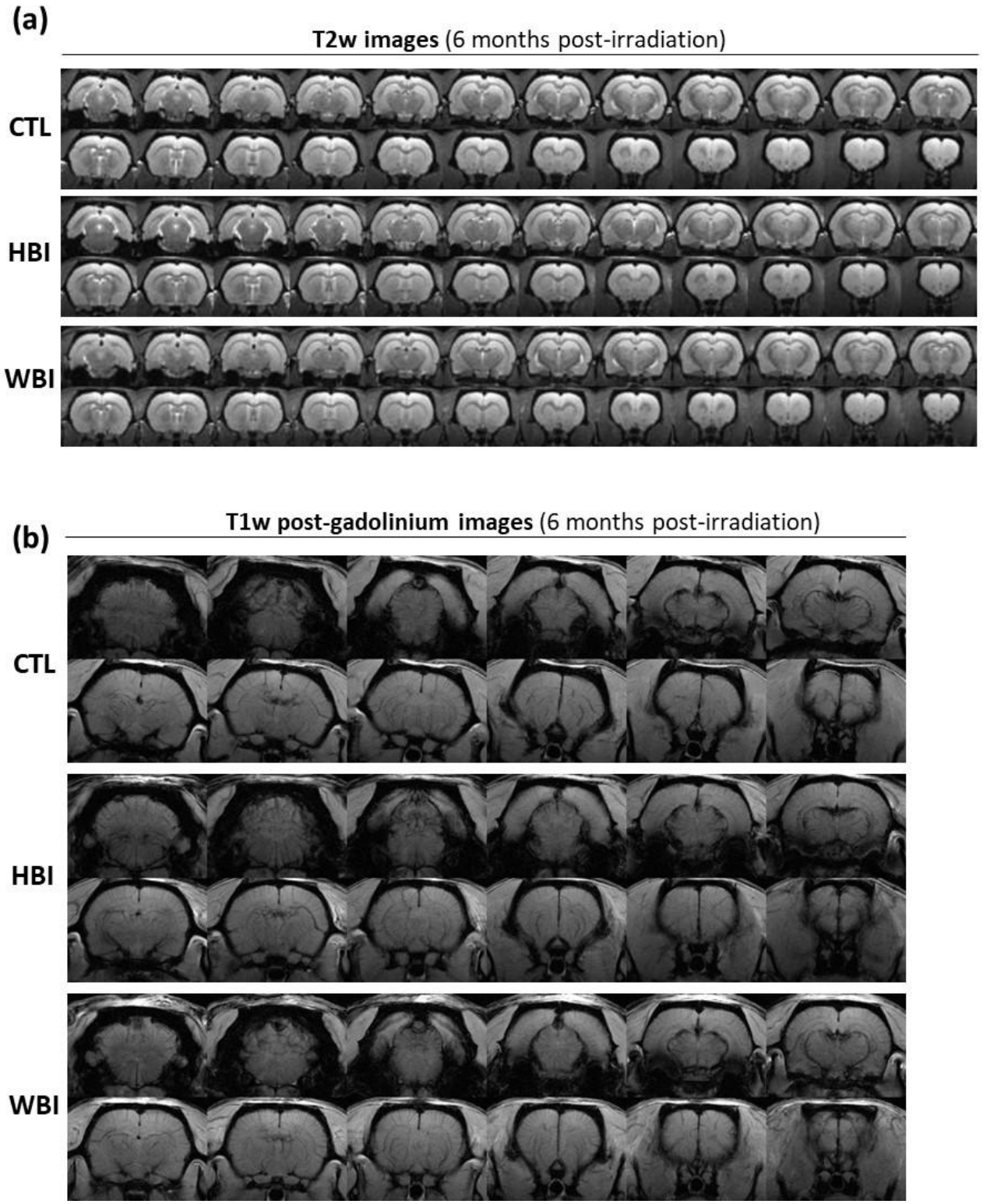

Supplementary Figure 2: Qualitative evaluation of brain edema and necrosis. (a) Representative T2-weighted (T2w) images of the whole brain acquired at 6 months in non-irradiated group (CTL), hemispheric brain irradiation (HBI) or whole-brain irradiation (WBI). **(b)** Representative T1-weighted (T1w) post-gadolinium images of the whole brain acquired at 6 months in CTL, HBI or WBI groups.

Supplementary Figure 3

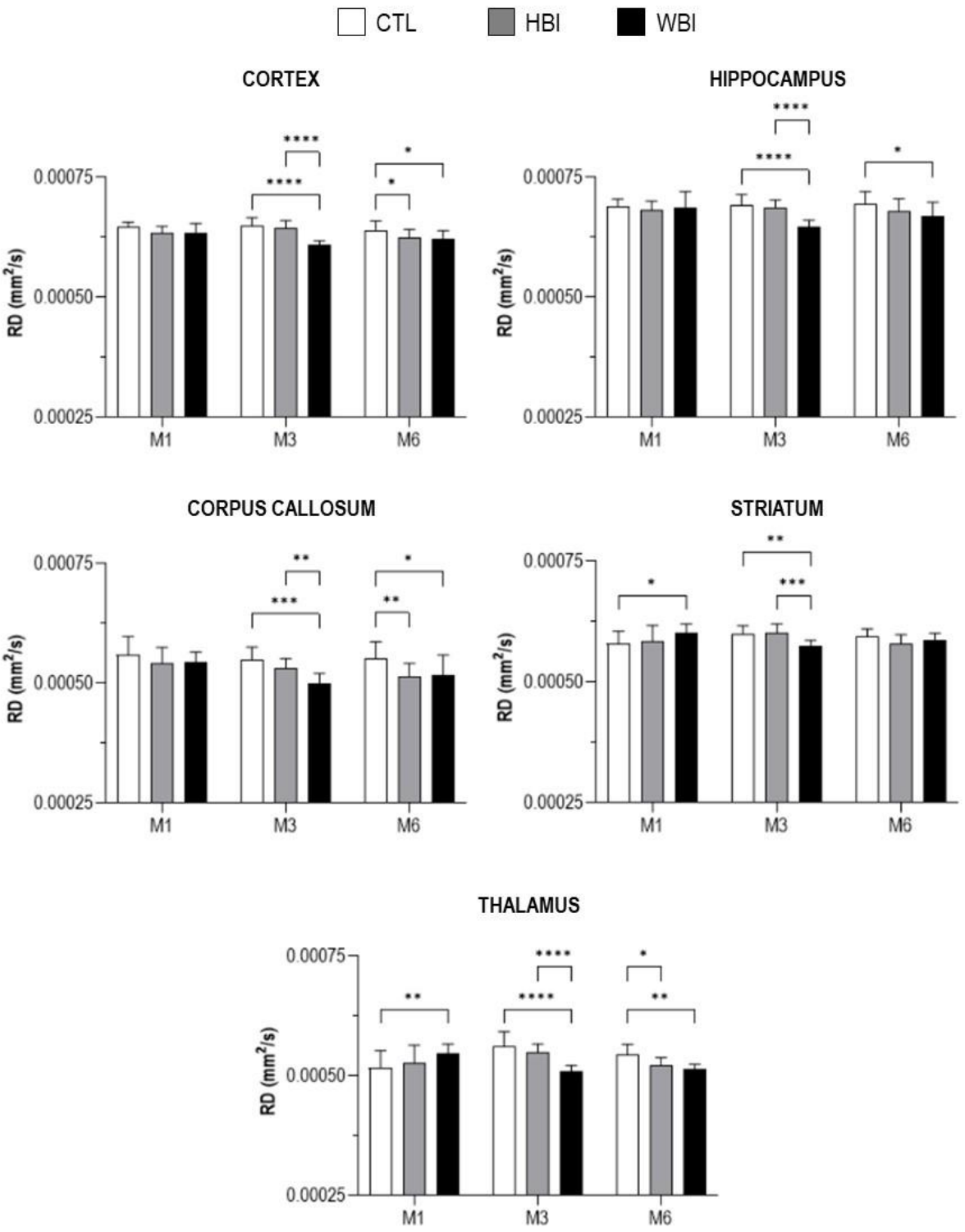

<u>Supplementary Figure 3</u>: Assessment of brain microstructure evolution following hemispheric or whole-brain irradiation by radial diffusivity (RD). Quantitative representation of RD values in the right hemisphere in 5 regions of interest (*i.e.* cortex, hippocampus, corpus callosum, striatum and thalamus) at 1-, 3- and 6-months post-irradiation. RD values were measured for non-irradiated rats (CTL: white, n=9), rats submitted to right hemispheric brain irradiation (HBI: gray, n=10-11) or whole-brain irradiation (WBI: black, n=8-10). Mean + SD; two-way ANOVA followed by Fisher's LSD test: * $p < 0.05$, ** $p < 0.01$, *** $p < 0.001$, **** $p < 0.0001$.

Supplementary Figure 4

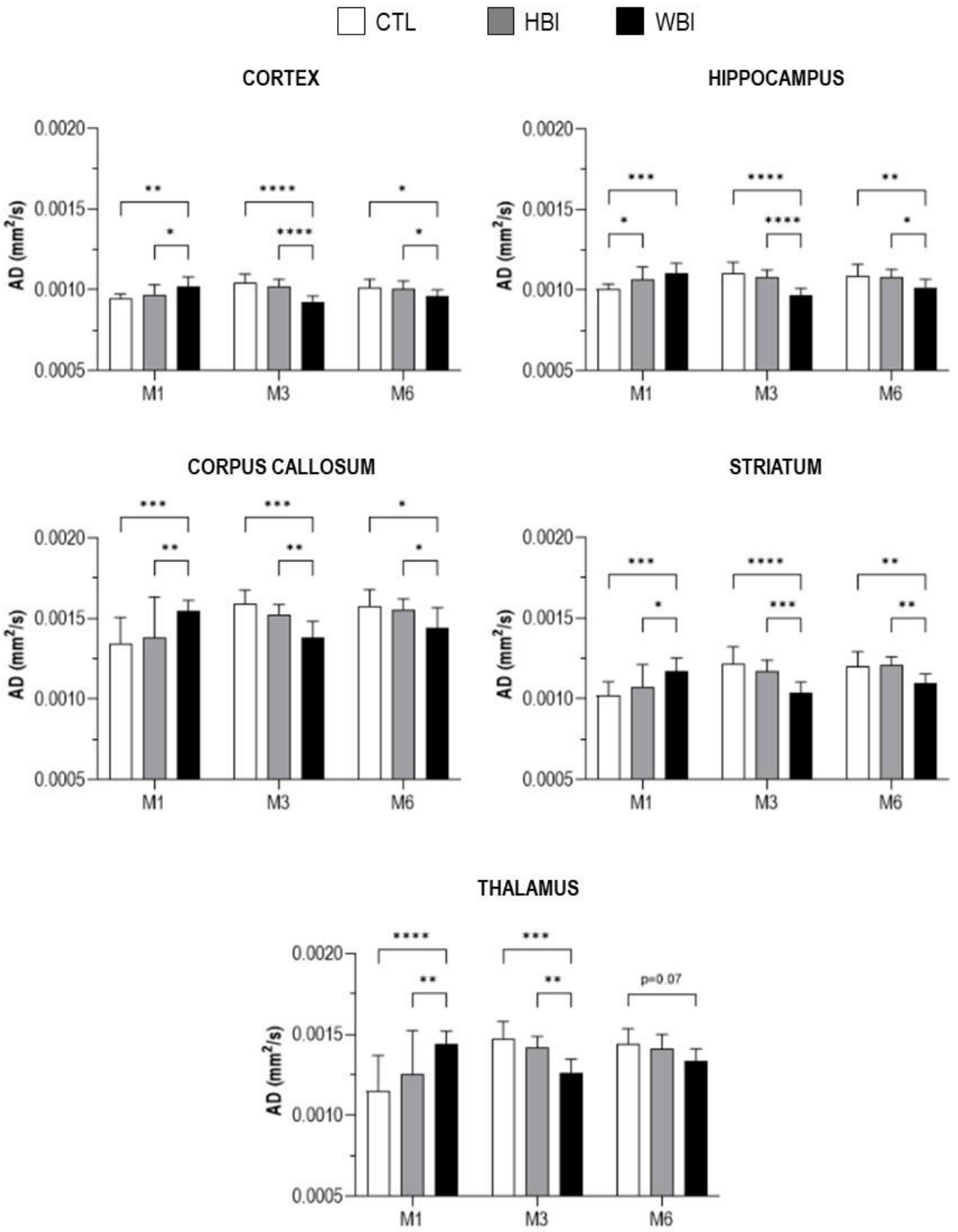

<u>Supplementary Figure 4</u>: Assessment of brain microstructure evolution following hemispheric or whole-brain irradiation by axial diffusivity (AD). Quantitative representation of AD values in the right hemisphere in 5 regions of interest (*i.e.* cortex, hippocampus, corpus callosum, striatum and thalamus) at 1, 3- and 6-months post-irradiation. AD values were measured for non-irradiated rats (CTL: white, n=9), rats submitted to right hemispheric brain irradiation (HBI: gray, n=10-11) or whole-brain irradiation (WBI: black, n=8-10). Mean + SD; two-way ANOVA followed by Fisher's LSD test: * $p < 0.05$, ** $p < 0.01$, *** $p < 0.001$, **** $p < 0.0001$.

Supplementary Figure 5

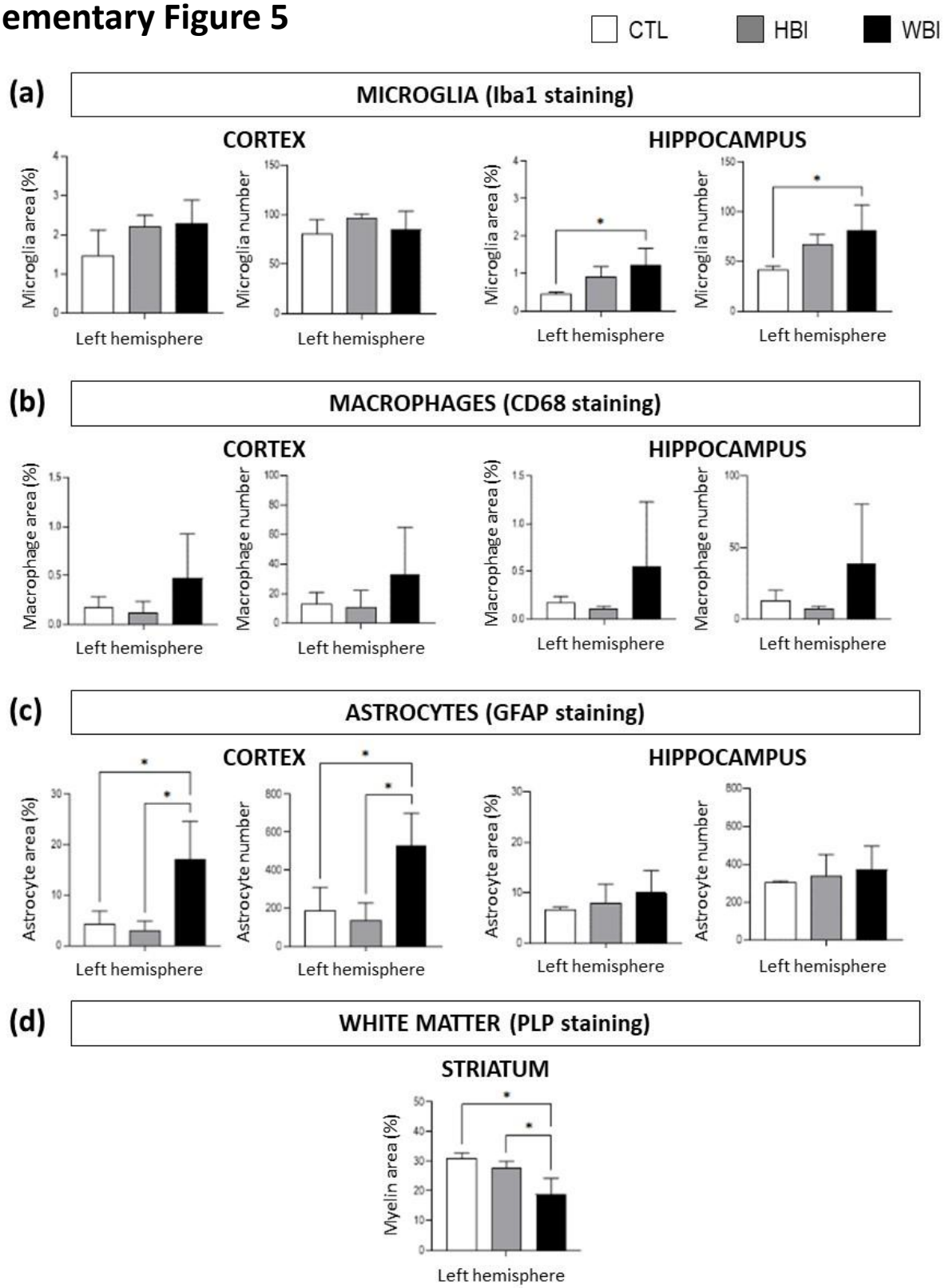

Supplementary Figure 5: Effects of hemispheric or whole-brain irradiation on microglia/macrophages, astrocytes and white matter in the left hemisphere. Quantification in the cortex and the hippocampus in the left hemisphere (contralateral side) in non-irradiated (CTL group), only right hemisphere irradiated (HBI group) and whole-brain irradiated (WBI) rats. Quantification of **(a)** microglia with Iba1 immunostaining, **(b)** macrophages with CD68 immunostaining, **(c)** astrocytes with GFAP immunostaining and **(d)** myelin with PLP immunostaining. Mean + SD, n=3 rats for each experimental group and each immunostaining, one-way ANOVA followed by Fisher's LSD test: * $p < 0.05$.

Supplementary Figure 6

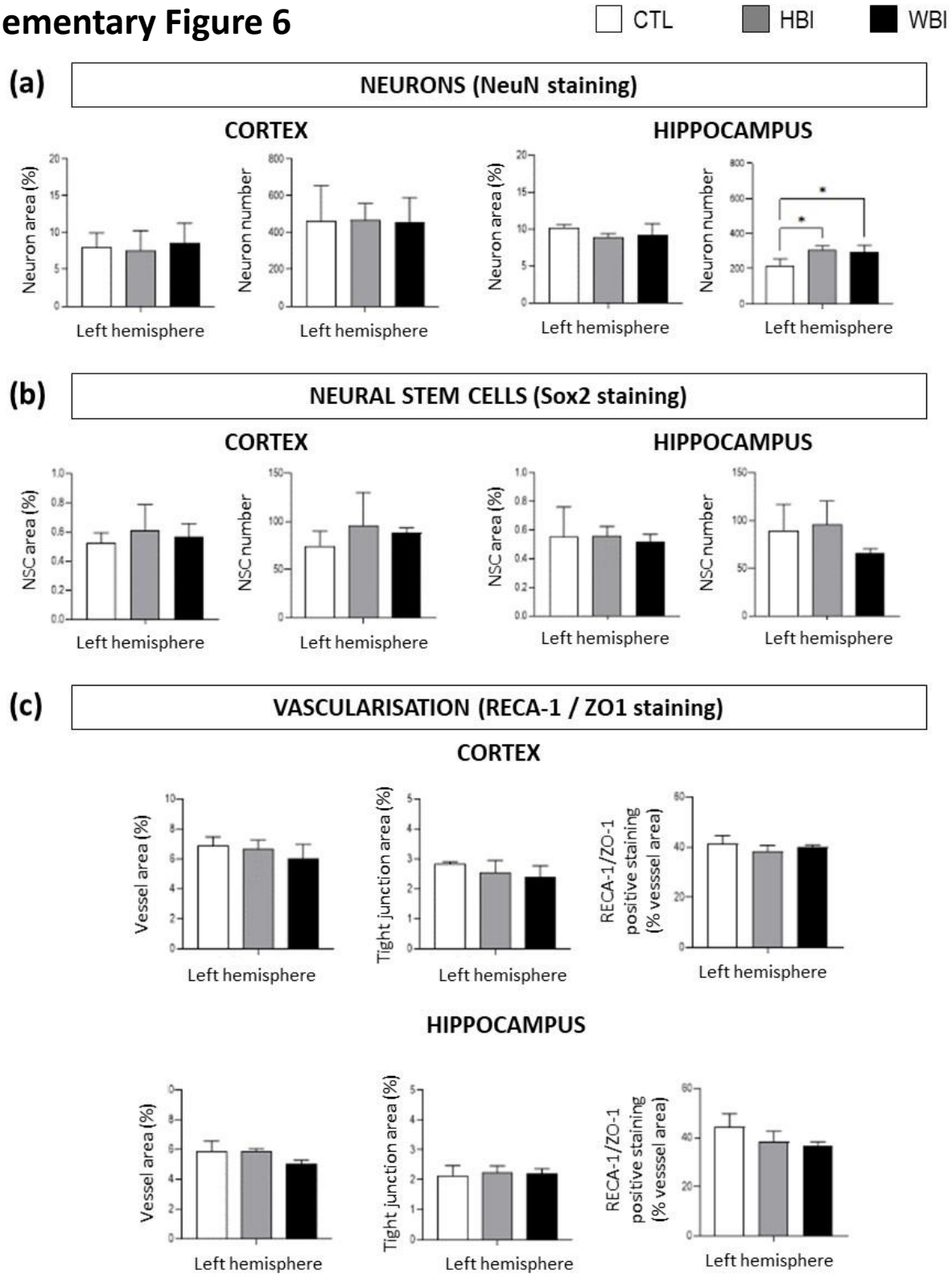

<u>Supplementary Figure 6</u>: Effects of hemispheric or whole-brain irradiation on mature neurons, neural stem cells and vascularization in the left hemisphere. Quantification in the cortex and the hippocampus in the left hemisphere (contralateral side) in non-irradiated (CTL group), only right hemisphere irradiated (HBI group) and whole-brain irradiated (WBI) rats. Quantification of **(a)** mature neurons with NeuN immunostaining, **(b)** neural stem cells (NSC) with Sox2 immunostaining and **(c)** brain vascularization by staining of endothelial cells with anti-RECA-1 antibody and staining of tight junctions with anti-ZO-antibody to assess vessel area and BBB integrity respectively. Mean + SD, n=3 rats for each experimental group and each immunostaining, one-way ANOVA followed by Fisher's LSD test: * $p < 0.05$.